

# Loop models and their critical points

Paul Fendley

Department of Physics, University of Virginia,  
Charlottesville, VA 22904-4714 USA  
fendley@virginia.edu

Loop models have been widely studied in physics and mathematics, in problems ranging from polymers to topological quantum computation to Schramm-Loewner evolution. I present new loop models which have critical points described by conformal field theories. Examples include both fully packed and dilute loop models with critical points described by the superconformal minimal models and the  $SU(2)_2$  WZW models. The dilute loop models are generalized to include  $SU(2)_k$  models as well.

## I. INTRODUCTION

The statistical mechanics of loop models have been studied extensively for decades. These models describe physical systems, and also provide fundamental problems in mathematics. Major progress has been made recently in understanding their properties. This is especially true when the loops are embedded in two dimensions, where the extensive variety of theoretical tools available have made many computations not only exact, but rigorous as well.

In a loop model, the degrees of freedom are one-dimensional. These “loops” may branch and touch, but are not allowed to have ends. The partition function is of the form

$$Z = \sum_{\mathcal{L}} w(\mathcal{L}) t^{L(\mathcal{L})}. \quad (1)$$

This sum is made precise by defining the loops to live on the links of some lattice. Then  $\mathcal{L}$  labels a single loop configuration where the loops have total length  $L(\mathcal{L})$ , i.e.  $L$  links of the lattice are covered by a loop. The parameter  $t$  is therefore a weight per unit length, which in this paper will usually be tuned to a special value which makes the behavior critical. Different loop models are distinguished by the choice of the weight  $w(\mathcal{L})$ . Here it is required that  $w(\mathcal{L})$  depends only on *topological* properties of a given configuration  $\mathcal{L}$ . Topological weights can depend on the number of loops, how many times loops touch, and more intricate properties like the number of ways of coloring a given graph.

A simple and famous example of a loop model goes under a variety of names: “ring polymers”, “closed self-avoiding random walks”, or the “ $O(n)$  loop model” [1]. Here the loops are defined so that they do not branch and do not touch each other, i.e. if two or more loops touch the same point, a prescription for resolving them must be given. A typical configuration is displayed in figure 1; the lattice is rotated by 45 degrees for later convenience. A simple topologically-invariant quantity is the number of loops  $\mathcal{N}$  in a given loop configuration  $\mathcal{L}$ . The  $O(n)$  loop model is then defined by taking

$$w(\mathcal{L}) = n^{\mathcal{N}} \quad (2)$$

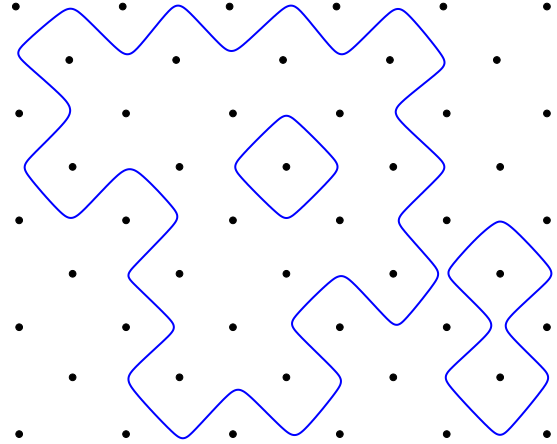


FIG. 1: A typical configuration in the  $O(n)$  loop model on the square lattice; the sites drawn are on the dual lattice.

for some parameter  $n$ . A single loop/walk/polymer can be obtained by requiring  $n \rightarrow 0$ . An interesting variation on this model comes from requiring that every site of the lattice be visited by at least one loop. Such loops are called *fully packed*, and their critical points are very different from those of the  $O(n)$  model without this requirement [1, 2, 3].

Many well-known models of statistical mechanics can be expressed in terms of loops. A simple example is the Ising model in two dimensions. A loop configuration is found from each spin configuration simply by writing the domain walls separating regions of up and down spins. A given loop configuration corresponds to two spin configurations, since flipping all the spins does not change the domain walls. These Ising loops/domain walls can touch, but do not have ends, and cannot branch: there must be even number of links with loops at any lattice site. The weight per unit length  $t = e^{-2K}$  for the usual Ising nearest-neighbor coupling  $K = J/(k_B T)$ , while the topological weight  $w(\mathcal{L}) = 1$  for all allowed  $\mathcal{L}$ .

It is essential to note that statistical-mechanical models defined by (1) do not necessarily have local Boltzmann weights. Since a single loop can be arbitrarily large, topological properties like the number of loops are defined non-locally. In some cases, there is a model with

local Boltzmann weights with the same partition function. Generically, these Boltzmann weights are complex, and so the theory is non-unitary. In some special cases like the  $O(n)$  model with  $n = 2 \cos(\pi/(k+2))$  with  $k$  a positive integer, a local model with positive Boltzmann weights does exist.

Interesting questions in both physics and mathematics arise in the continuum limit. In this limit one can apply a variety of powerful field-theory methods to understand the phase diagram and compute properties at and near critical points. One major breakthrough in the study of two-dimensional loop models came with the invention of Coulomb-gas methods (see [1] for a review). These methods allowed non-trivial critical points to be found, and many critical exponents to be computed exactly, under a well-motivated set of assumptions about the behavior of the loops in the continuum limit. Further progress in understanding these critical points came with the introduction of conformal field theory [4]. When a critical point in a loop model is in the same universality class as a known conformal field theory, then not only can critical exponents be found, but correlators computed exactly [5].

A remarkable recent development in the study of loop models came with the introduction of Schramm-Loewner evolution (SLE) [6]. SLE provides a novel way of formulating conformal field theory geometrically. Among many other things this gives a direct way of deriving which conformal field theory describes certain loop models; sometimes the correspondence can even be proved rigorously.

Another reason for recent interest in loop models comes from the search for quantum theories with quasiparticles obeying non-abelian statistics. Aside from their intrinsic interest, such quasiparticles could make up the “qubits” of a topological quantum computer [7, 8]. One of the few types of models exhibiting such quasiparticles are quantum theories whose Hilbert space has basis elements consisting of loops in two dimensions. The ground-state wave function is a sum over all such loops, so that ground-state correlators in the quantum theory are identical to those in a two-dimensional classical loop model like the ones studied here.

Despite all the recent activity and progress, not many different types of loop models have been studied in depth. One reason is that many loop models do not have critical points. For example, the  $O(n)$  loop model has a critical point only when  $n \leq 2$ . There are many interesting and simple conformal field theories which have no known description in terms of loops. Moreover, for all the successes of the SLE approach, it applies only to a very small set of conformal field theories.

The purpose of this paper is to develop a general procedure for finding a two-dimensional loop model with a critical point and a corresponding conformal field theory description. This procedure yields a number of new models whose geometric properties should be understandable by using conformal field theory, and will hopefully prove

useful for SLE and for topological quantum computation. For example, the loop models described here may provide a way of geometrically interpreting the SLE processes described in [9].

The strategy is to start with classical lattice models whose degrees of freedom are not loops, but rather are *heights*, integer-valued variables on the sites of the square lattice. The Boltzmann weights are local and positive, so any field theories obtained from taking the continuum limit of these models are unitary. The height models utilized are *integrable*, which makes it possible to find a variety of exact results. Choosing these models judiciously makes it possible to

1. Locate critical points within the lattice model, and find the conformal field theory describing the continuum behavior of each critical point.
2. Re-express the partition function in terms of loop degrees of freedom, instead of heights, just as discussed for the Ising model above.

Putting these two together gives a loop model whose critical point is described by a known conformal field theory. Typically, this sort of precise mapping will apply only when the topological weight  $w(\mathcal{L})$  can be expressed in terms of local quantities. However, once this map is made, the extension to more general non-unitary cases is obvious.

There are two types of loop models to be discussed here. *Fully packed* loop models have the requirement that (at least) one loop touches every site on the lattice. Models which do not have this requirement are referred to as *dilute*. The latter naming is somewhat cavalier: the critical points of interest typically are believed to describe a phase transition between a dilute phase (where only a set of measure zero of the sites are touched on average by a loop), and a dense phase (where only a set of measure zero of the sites are not touched by a loop). Nevertheless, since at the critical point the loop density is still zero (like the magnetization in the Ising model), I will persist with the name.

The dilute and fully packed loop models arise here in very different ways. The fully packed models are found by expressing the transfer matrix of a lattice height model in terms of the generators of an algebra, and then finding a loop representation of the same algebra. It is then possible to define a loop model which has the identical partition function. The dilute models arise more indirectly: by studying the ground states of the Hamiltonian associated with the (same) lattice height model, one can infer what the domain walls are. Like in the Ising model, the loops are the domain walls. This argument is not rigorous like that for the fully packed loops, but substantial consistency checks are made using exact results from the corner transfer matrix and the scattering matrix.

The outline of the rest of the paper is as follows. In section II, I present the main results. In section III, I review how the “minimal models” of conformal field theory are

related to both dilute and fully packed loop models. In section IV, I introduce height models which have critical points described by the superconformal minimal models and  $SU(2)_2$  conformal field theory. There these height models are used to define fully packed loop models whose topological weight is given by a chromatic polynomial. In section V, dilute loop models are found which have these critical points, and then generalized to include  $SU(2)_k$  as well. In appendix A the relevant conformal field theories are reviewed briefly. In appendix B, the appropriate boundary conditions for the lattice models are discussed, while some technical details on the BMW algebra are collected in appendix C.

## II. THE LOOP MODELS AND THE RESULTS

In this section I introduce the dilute and fully packed loop models studied in this paper, and describe their critical points. The following sections are then devoted to explaining and deriving these results.

### A. Dilute loops

The dilute-loop model discussed in this paper is a generalization of the  $O(n)$  loop model with two types of loops. The two types are strongly coupled: each link containing one kind of loop must also contain the other. A configuration is displayed in figure 2, where the two types of loops are represented by solid and dashed lines. The loops are drawn across the diagonals of the plaquettes of the square lattice.

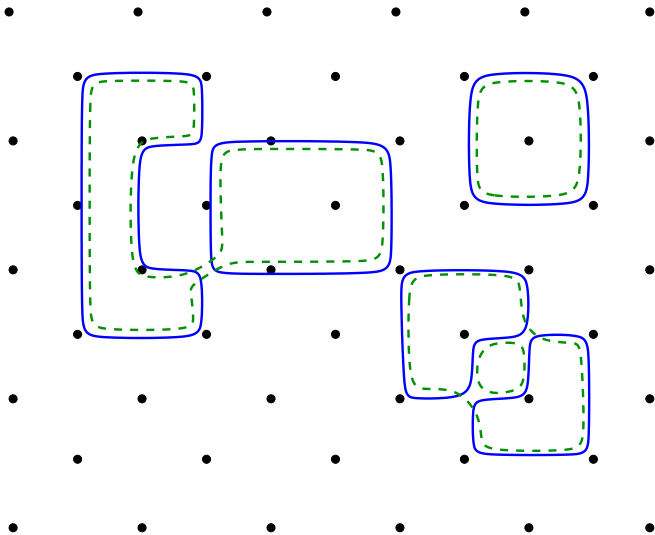


FIG. 2: A typical configuration in the new dilute loop model.

In both this model and the  $O(n)$  model there may be two loops coming into the same point on the lattice, and it is required that they do not cross. The new model is

distinguished from the  $O(n)$  model by how the loops are resolved when they potentially cross at the *center* of a plaquette. In the new models, it is required that loops of *each type* do not cross. Loops of different types may cross; the four different possibilities are illustrated below in figure 15.

Topologically-invariant quantities of such loop configurations are the numbers  $\mathcal{N}$  and  $\mathcal{M}$  of each kind of loop, and  $\mathcal{C}$ , the number of plaquettes with a resolved potential crossing at their center. In figure 4 these are  $\mathcal{N} = 5$ ,  $\mathcal{M} = 4$ , and  $\mathcal{C} = 4$ . The topological weight is

$$w(\mathcal{L}) = n^{\mathcal{N}} m^{\mathcal{M}} b^{\mathcal{C}} \quad (3)$$

where  $n$ ,  $m$  and  $b$  are parameters. For  $m = b = 1$ , this weight reduces to that of the  $O(n)$  model. It is convenient to parametrize  $n$  and  $m$  by

$$\begin{aligned} n &= 2 \cos\left(\frac{\pi}{p-k+1}\right), \\ m &= 2 \cos\left(\frac{\pi}{k+2}\right). \end{aligned} \quad (4)$$

I will argue that with appropriate boundary conditions, these dilute loop models have a critical point described by a unitary conformal field theory when  $p$  and  $k$  are integers with  $p > k + 1$  and  $k > 1$ . These conformal field theories are called coset models, and are described briefly in appendix A. The  $k = 1$  case reduces to the  $O(n)$  model, which is well known to be described by the conformal minimal models [5]. For  $k = 2$ , the conformal field theories are the superconformal minimal models, whereas for  $p \rightarrow \infty$  ( $n \rightarrow 2$ ), they are the  $SU(2)_k$  Wess-Zumino-Witten models. It is natural to conjecture that this loop model has a critical point when  $n \leq 2$  and  $m \leq 2$ , although for  $p$  and  $k$  outside these special values, the corresponding conformal field theories will be non-unitary.

### B. Fully packed loops

A fully packed version of the  $O(n)$  loop model is illustrated in figure 3. In this version the loops cover every link of the square lattice. The only degree of freedom is how the loops are resolved at each site of the lattice: there are two possible resolutions which do not allow crossings. The topological weight is then

$$w_F(\mathcal{L}) = (\sqrt{Q})^{\mathcal{N}} \quad (5)$$

when there are  $\mathcal{N}$  of these loops. The weight per loop is labeled  $\sqrt{Q}$  here because for weight per unit length  $t = 1$  and appropriate boundary conditions, this model is equivalent to the  $Q$ -state Potts model at its self-dual point. This is shown using the high-temperature expansion of the Potts model [10, 11], which will be reviewed in section III A. The Potts self-dual point is critical when  $Q \leq 4$ , so that the critical point occurs for a

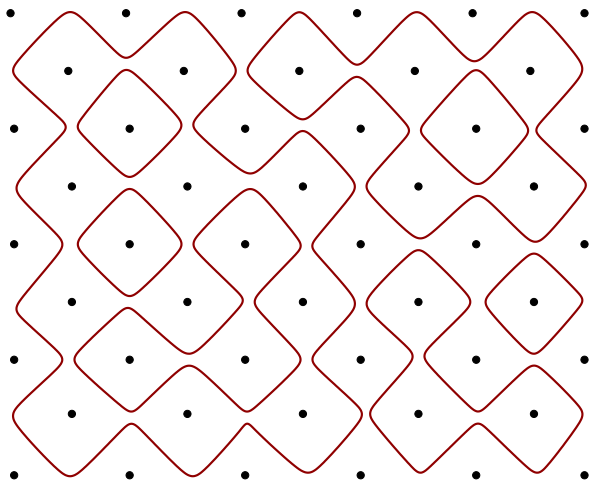


FIG. 3: A typical configuration in a fully packed  $O(n)$  loop model

weight per loop  $\leq 2$ , just like the dilute  $O(n)$  models. Also like the dilute  $O(n)$  models, the continuum limit of the critical Potts models are described by the minimal models of conformal field theory when  $Q$  takes on special values. One obtains the  $p$ th minimal model when  $\sqrt{Q} = 2 \cos(\pi/(p+1))$  with  $p$  integer; note the shift of  $p$  relative to the dilute value found in (4) with  $k = 1$ . This critical point is often called the *dense* critical point of the  $O(n)$  loop model [1, 2].

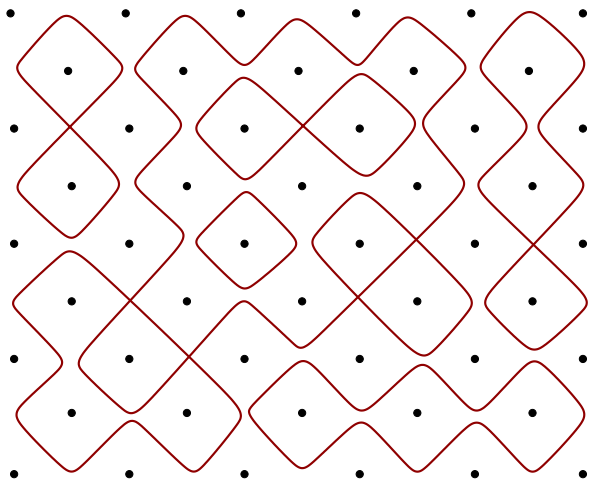


FIG. 4: A typical configuration in the fully packed  $k = 2$  model

In terms of the more general coset conformal field theories with central charge (A3), the minimal models and hence the dense critical points have  $k = 1$ . In section IV I derive fully packed loop models which have critical points corresponding to the  $k = 2$  case, the superconformal minimal models. A typical configuration in this fully packed model is illustrated in figure 4. There are three allowed configurations for each vertex, the two ways of

resolving the lines so that they do not cross, and a third, which I call the “intersection”. Since these intersections are not resolved, the configurations do not really form loops, but for lack of a better name, I still call the degrees of freedom loops.

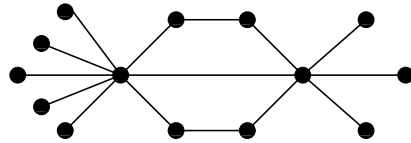


FIG. 5: The dual graph for the loop configuration in figure 4

The topological weight of the model is not defined by resolving the intersections to make the configurations into non-crossing loops. Instead, it is given in terms of the *chromatic polynomial*. To define the chromatic polynomial, it is first useful to note that the loops divide the plane into different regions. These regions can be thought of as countries on a map, and a  $Q$ -coloring gives each country one of  $Q$  colors, such that adjacent countries must have different colors. If two regions touch only at a point (or any countable set of points), they are not adjacent. This is convenient to formulate in terms of the dual graph. Each region corresponds to a vertex on the dual graph, and two vertices are joined by an edge if the corresponding regions are adjacent. The dual graph for the loop configuration in figure 4 is illustrated in 5. Note that the dual graph only depends on the topology of the original loop configuration. The number of  $Q$ -colorings  $\chi_Q(\mathcal{L})$  of the dual graph is the number of ways of assigning  $Q$  colors to each vertex with the constraint that any vertices joined by an edge must be a different color.

There exists no closed-form formula for the number of colorings of a general graph. However,  $\chi_Q$  can be determined recursively. Consider two vertices connected by an edge  $l$  (i.e. two regions sharing a boundary in the original picture). Then define  $\mathcal{D}_l\mathcal{L}$  to be the graph with the  $l$  edge deleted, and  $\mathcal{C}_l\mathcal{L}$  to be the graph with the two vertices connected by  $l$  joined into one. Then it is simple to prove that

$$\chi_Q(\mathcal{L}) = \chi_Q(\mathcal{D}_l\mathcal{L}) - \chi_Q(\mathcal{C}_l\mathcal{L}). \quad (6)$$

In the dual graph of  $\mathcal{L}$  the two vertices connected by  $l$  must be colored differently, while in  $\mathcal{D}_l\mathcal{L}$ , they may be the same, Thus  $\chi_Q(\mathcal{D}_l\mathcal{L}) \geq \chi_Q(\mathcal{L})$ , and the number of colorings overcounted is  $\chi_Q(\mathcal{C}_l\mathcal{L})$ . The number of colorings can then be determined by using this recursion relation to remove edges and vertices from  $\mathcal{L}$  until it is a sum of terms which have no edges at all. A term with  $\mathcal{V}$  vertices and no edges has  $\chi_Q = Q^{\mathcal{V}}$ . An illuminating example is the case where there are no intersections, so that the configurations really are loops. The dual graph is then tree-like (it has no faces). Vertices at the ends of the tree can be removed one by one using (6), with each vertex being removed giving a factor  $Q - 1$ . This yields

$\chi_Q = Q(Q-1)^{\mathcal{V}-1}$  for a tree with  $\mathcal{V}$  vertices. Using the recursion relation (6) gives for the loop configuration in figure 4 and the dual graph in figure 5

$$\chi_Q = Q(Q-1)^9(Q^2 - 3Q + 3)^2.$$

Repeatedly applying the recursion relation gives  $\chi_Q(\mathcal{L})$  as a polynomial in  $Q$  of order  $\mathcal{V}$ . This is known as the chromatic polynomial, and depends only on the dual graph of  $\mathcal{L}$ . This polynomial provides a well-defined extension of  $\chi_Q$  away from  $Q$  integer. The fully packed loop model is therefore uniquely defined for any  $Q$  with topological weight

$$w(\mathcal{L}) = \chi_Q(\mathcal{L})(\sqrt{Q} + 1)^{-\mathcal{N}_X}. \quad (7)$$

$\mathcal{N}_X$  is the number of intersections; the factor involving it arises from the detailed analysis below. The full partition function is given by using this topological weight with (18), where the weight per unit length of loop is  $t = 1$ . The sum is over all loops on the square lattice such that each plaquette has one of the three configurations drawn in figure 12.

In section IV B I prove that the loop model with topological weight (7) has a critical point described by the  $p$ th superconformal minimal model (i.e. those in (A2) with  $k = 2$ ), when

$$Q = 4 \cos^2 \left( \frac{\pi}{p+1} \right). \quad (8)$$

These fully packed models presumably remain critical for all real  $p$ , but are described by a non-unitary conformal field theory for  $p$  non-integer.

This loop model is very similar to that of [12], which arises from the low-temperature expansion of the  $Q$ -state Potts model. The topological weight is given by the chromatic polynomial. However, the loops there are dilute, not fully packed, and intersections with three lines coming out are allowed there. As a result, the critical point there is described by the conformal minimal models instead of the superconformal minimal models.

This is not the only fully packed loop model which has critical points corresponding to the superconformal minimal models. One based on non-intersecting loops on the ‘‘copper-oxide’’ lattice will also be briefly discussed below.

### III. THE $O(n)$ LOOP MODELS

The strategy of this paper is to use known integrable lattice models to find loop models with critical points described by conformal field theories. In this section this strategy is used to connect the  $O(n)$  loop models with the minimal models of conformal field theory. None of the results in this section are new, but possibly some of the arguments are. After introducing the lattice models, the two different possible loop expansions are derived.

Even though both loop expansions come from the same lattice model, they arise in very different ways. The fully packed loops arise by rewriting the model in terms of an algebraic formulation of the transfer matrix, which in most contexts is a high-temperature expansion. Dilute loops arise from a domain-wall expansion, which is a low-temperature expansion.

#### A. RSOS lattice models

The lattice models here are the ‘‘restricted-solid-on-solid’’ (RSOS) models introduced by Andrews, Baxter and Forrester [13]. The degrees of freedom are integer-valued heights  $h_i$  on each site  $i$  of the square lattice. There are two types of restriction. The first is that  $h_i$  only takes a finite number of possibilities, which are numbered from  $1 \dots p$  for some integer  $p$ . The second is that heights on adjacent sites must differ only by 1, i.e.  $|h_i - h_j| = 1$  for  $i$  and  $j$  nearest neighbors. The latter restriction will be modified for the models in later sections. In order to utilize crucial exact results, I study only height and loop models on the square lattice. However, frequently (but not always), one obtains similar results on different two-dimensional lattices.

The  $p = 3$  case is the Ising model: on one sublattice the height must always be 2, so that on the other sublattice the heights 1 and 3 play the roles of the  $+$  and  $-$  Ising spins. The  $p = 4$  RSOS model is known as the hard square model [11]; a typical configuration is illustrated in figure 9 below.

The RSOS models are interesting and useful because for special choices of the Boltzmann weights, they are integrable. Integrability allows a number of important physical quantities to be computed exactly, under a set of standard analyticity assumptions. Critical points and the associated exponents can be found using a powerful technique called the corner transfer matrix [11]. Conformal field theory also provides a list of critical exponents associated with critical points. By comparing the two lists, one can usually identify the conformal field theory describing the continuum limit of any critical point in an RSOS model. For these RSOS models, there are two known critical points for each value of  $p > 3$ . This paper is concerned with just one of them, the one separating regimes III and IV in the nomenclature of [13]. This critical point is described by the  $p$ th minimal model, with central charge given by (A1) [16].

Finding the loop models associated with this RSOS model and hence the conformal minimal models requires analyzing the Boltzmann weights in detail. The weights contains nearest-neighbor and next-nearest-neighbor interactions, so the total weight can be written as a product of weights assigned to the four heights around each square plaquette. Such a model is called ‘‘interaction round a face’’ [11]. The transfer matrix  $T_{h,h'}$  is defined to act across the diagonals of the lattice, as illustrated in figure 6. It therefore acts on a zig-zag row of heights  $h_i$ ,

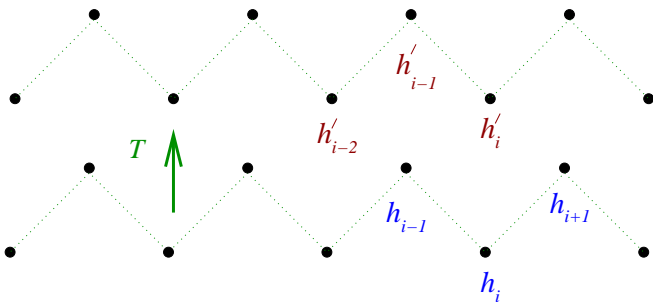


FIG. 6: How the transfer matrix acts

$i = 0 \dots 2N$ , taking it to the next row, labeled by  $h'_i$ . It can be broken into pieces  $\mathcal{T}_i$ , which depend only on the heights around a square, and can change  $h_i$  to  $h'_i$ . Then  $T_{h,h'}$  can be written in the form

$$T = \mathcal{T}_1 \mathcal{T}_3 \dots \mathcal{T}_{2N-1} I_0 \mathcal{T}_2 \mathcal{T}_4 \dots \mathcal{T}_{2N-2} I_{2N} \quad (9)$$

where the identity matrix  $I_i = \delta_{h_i h'_i}$ . For the RSOS critical point of interest here, we have

$$\mathcal{T}_i = I_i + x e_i \quad (10)$$

where  $x$  is a parameter, and the elements of the matrix  $e_i$  for  $i$  even are [13, 14]

$$e_i = \delta_{h_{i-1} h_{i+1}} \frac{\sqrt{[h_i]_q [h'_i]_q}}{[h_{i+1}]_q} \prod_{j \text{ even}, j \neq i} I_j \quad (11)$$

where

$$[h]_q \equiv (q^h - q^{-h}) / (q - q^{-1}), \quad q \equiv e^{\pi i / (p+1)}.$$

Acting with  $e_i$  therefore allows the height on the  $i$ th site to change when  $h_{i-1} = h_{i+1}$ . For  $i$  odd, the matrix  $e_i$  is essentially the same:

$$e_i = \delta_{h'_{i-1} h'_{i+1}} \frac{\sqrt{[h_i]_q [h'_i]_q}}{[h'_{i+1}]_q} \prod_{j \text{ odd}, j \neq i} I_j \quad (12)$$

The RSOS transfer matrix written in this form exhibits an interesting and important algebraic structure: the  $e_i$  generate the *Temperley-Lieb algebra* [15]. It is straightforward to check that they satisfy

$$\begin{aligned} e_i^2 &= (q + q^{-1}) e_i, \\ e_i e_{i\pm 1} e_i &= e_i, \\ e_i e_j &= e_j e_i \quad (|j - i| \geq 2). \end{aligned} \quad (13)$$

This algebra first arose in studies of the  $Q$ -state Potts model, whose transfer matrix also can be written in the form (9,10), with the  $e_i$  satisfying the same algebra (13) with  $q + q^{-1} = \sqrt{Q}$ . Since then, it has been shown how to write many other lattice models in this same form.

Writing a transfer matrix in terms of the Temperley-Lieb generators is exceptionally useful because many

properties of the model follow solely from the algebra, and are independent of the representation of the  $e_i$ . With appropriately-chosen boundary conditions, the partition function is independent of representation. This is shown for a two-dimensional surface with the topology of a sphere in the appendix B, while detailed discussions for the cylinder and torus can be found in [17, 18]. In many considerations, understanding the boundary conditions precisely is very important; for example, the central charge of the continuum conformal field theory depends on them. For the results here, the details of the boundary conditions are not particularly important – what is of main importance is that appropriate ones exist.

## B. Fully packed loops

This construction of the fully packed loop model associated with each critical RSOS model is virtually identical to that of the fully packed loop model for the Potts model [10, 11]. This is easiest to do by using a graphical representation of the Temperley-Lieb generators [17].

Fully packed loop configurations are not in one-to-one correspondence with those of the height or Potts model. Rather, for each height configuration, the product in (9) is expanded out by using (10). One obtains either the identity  $I$  or the Temperley-Lieb generator  $e$  for each plaquette, so that for  $\mathcal{P}$  plaquettes there are  $2^{\mathcal{P}}$  terms. Each term can be graphically represented by drawing one of the two pictures in figure 7 for each plaquette, depending on whether  $I$  or  $e$  appeared for this plaquette. This gives a fully packed configuration of self-avoiding and mutually-avoiding loops on the dual square lattice. Every link of the dual lattice is covered by a loop, and at each vertex there are two possible ways of resolving the lines so that the loops do not cross. These properties can be preserved at the boundaries as well, as described in appendix B.

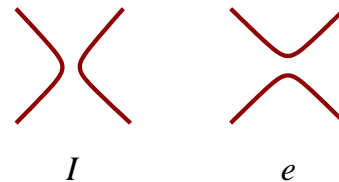


FIG. 7: The graphical representation of the Temperley-Lieb generators

To obtain the fully packed loop model, one must sum over the heights in the RSOS representation (or the spins in the Potts representation), leaving only the loops themselves as the degrees of freedom. The sum is not difficult to do directly in the RSOS representation [17] (or in the Potts representation [10, 11]), by using the explicit representation for  $e$ , as given in (11). It is more instructive, however, to not utilize the details of any explicit representation, but rather to exploit the properties



of the Temperley-Lieb algebra. In the transfer matrix, summing over heights amounts to multiplying the matrices defined by  $I_i$  and  $e_i$ . Therefore, the algebra itself can be represented graphically as in figure 8. From this it is apparent that small closed loops receive a weight  $q + q^{-1}$ . By using both relations, it is easy to check that *all* loops receive this same weight  $q + q^{-1}$ , no matter what their size (for details, see appendix B). Setting  $x = 1$  to make the model isotropic (invariant under 90-degree rotations) yields the fully packed  $O(n)$  loop model discussed in the introduction. The weight per loop is  $n = q + q^{-1} = 2 \cos[\pi/(p+1)]$  for the RSOS model, or  $n = \sqrt{Q}$  for the  $Q$ -state Potts model. The weight per unit length of loop  $t$  in this case is unimportant, because every link is covered by a loop.

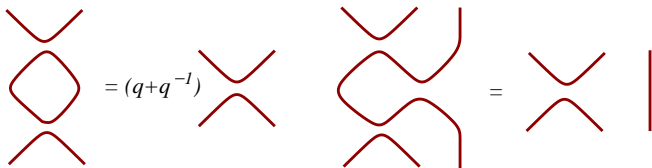


FIG. 8: The graphical representation of the Temperley-Lieb algebra

The  $O(n)$  loop model can of course be defined for any  $n$ , but is only critical for  $|n| \leq 2$ . This is shown by using the representation of yet another lattice model, the six-vertex model, in terms of the Temperley-Lieb algebra [11]. Another interesting thing to note is that even when  $|n| \leq 2$ , the conformal field theory is unitary only for integer  $p \geq 3$ . The representation (11) exists for any value of  $q = e^{i\pi/(p+1)}$ , but the only ones leading to real and positive Boltzmann weights for  $q + q^{-1} \leq 2$  occur at  $p$  integer.

### C. Domain walls in the RSOS model

The dilute  $O(n)$  loop model also has a critical point related to the conformal minimal models [5]. A way of showing this heuristically is to compare the Coulomb-gas description of the minimal models [5, 19] to that arising from the lattice model [1]. A way of showing this directly is to study a different series of integrable RSOS models known as the “dilute Temperley-Lieb” models [20, 21, 22]. In this section I give another method of relating the two, by using the RSOS models defined in section III A. This is the method which readily generalizes to  $k > 1$ .

It is useful to start by discussing how the dilute Temperley-Lieb models are related to the  $O(n)$  loop model [20, 21]. The dilute models are defined in terms of integer heights on the square lattice like the RSOS models discussed above in section III A, but the restriction on neighboring heights in the dilute models is relaxed to  $h_i - h_j = 0, \pm 1$ . The loops are simply the domain walls between different heights. The “dilute” in the name

refers to the fact that because  $h_i - h_j$  can vanish for near-est neighbors, there need not be domain walls on every link. Just drawing domain walls does not immediately make it into the  $O(n)$  loop model: there is no reason *a priori* why a region of heights 1 and 2 has the same weight as a region of heights 2 and 3. Nevertheless, when the Boltzmann weights are tuned appropriately, one can perform the sum over heights to leave a model consisting of self-avoiding and mutually-avoiding loops with weight  $n$  per loop [20]. By then doing a corner transfer matrix computation, one finds indeed that the continuum limit is described by a conformal minimal model, with the weight  $n$  per loop related to  $p$  by  $n = 2 \cos(\pi/p)$  (note the shift in  $p$  as compared to the fully packed case) [22].

The loops discussed in the remainder of this section can be thought of as domain walls for the RSOS model defined in section III A. However, they are not simply domain walls between differing heights, as they are in the dilute model. Instead, they are best thought of as domain walls between “ground states” in a 1+1-dimensional picture. Namely, one chooses a Euclidean time direction, and takes the continuum limit in the time direction to obtain a one-dimensional quantum Hamiltonian, and find its ground states. Excitations in the one-dimensional picture are then kinks, or defects, which separate regions comprised of the different ground states. The world lines of the kinks in 1+1 dimensions can be thought of as domain walls in the two-dimensional classical model. Obviously, this picture is heuristic, but below I will explain how to use it to develop exact results for the RSOS model into a precise conjecture for a dilute loop model.

A quantum Hamiltonian for the RSOS models is obtained in the limit  $x \rightarrow 0$ . One finds that the critical properties of the model are independent of  $x$ , as long as its sign is not changed. Thus taking  $x \rightarrow 0$  in (9) and (10) gives a quantum Hamiltonian acting in the same direction as the transfer matrix, i.e. across the diagonals of the lattice. It is (for  $x > 0$ )

$$H = - \sum_{i=1}^{2N-1} e_i . \quad (14)$$

This Hamiltonian acts on the “height chain”  $(h_0, h_2, \dots, h_{2N})$ .

Using (11), it is easy to find candidates for the ground states of (14). The matrix elements of  $e_i$  are positive when  $h_{i-1} = h_{i+1}$ , and vanish when  $h_{i-1} \neq h_{i+1}$ . Thus it is natural to expect that a ground state will be dominated by states that obey  $h_{i+1} = h_{i-1}$  for all  $i$ . The RSOS models defined in section III A have the restriction that  $h_i - h_{i-1} = \pm 1$  for all  $i$ . Thus potential ground states here are of the form  $(\dots, r, r+1, r, r+1, \dots)$ .

Finding which one or ones of these potential ground states dominates the actual ground state or states is in general an imposing problem. For the integrable Hamiltonian (14), however, it is possible to answer this question by using the corner transfer matrix technique [11, 13]. The result is that there is a ground state dominated by

each of the potential ground states. Thus this critical point is a multicritical point, where all the potential orderings coexist [16].

I illustrate this here in the simplest cases, and then in the next subsection III D explain how the general result follows from the corner transfer matrix. The simplest case is the Ising model, which has  $p = 3$ . The restriction that  $|h_i - h_{i+1}| = 1$  means that every other site on the chain (say the even sites) must be occupied by height 2. The odd sites are occupied by heights 1 and 3, which play the role of the spins  $\pm$  in the usual formulation of the Ising chain. Using the explicit matrix elements given in (11) means that  $-e_i$  for even  $i = 2j$  yields a potential energy which is  $-\sqrt{2}$  if  $h_{2j-1} = h_{2j+1}$ , and 0 for  $h_{2j-1} \neq h_{2j+1}$ . For odd  $i = 2j - 1$ ,

$$e_{2j-1} = \frac{1}{\sqrt{2}} \begin{pmatrix} 1 & 1 \\ 1 & 1 \end{pmatrix},$$

where the rows and columns are indexed by  $h'_{2j-1} = 1, 3$  and  $h_{2j-1} = 1, 3$  respectively. Rewriting the Hamiltonian in terms of the Pauli matrices  $\sigma^a(j)$  gives

$$H_{p=3} = -\frac{1}{\sqrt{2}} \sum_{j=1}^{N/2} [\sigma^z(j)\sigma^z(j+1) + t\sigma^x(j)]$$

where  $t = 1$ . This is exactly the ferromagnetic Ising spin chain;  $t = 1$  is the critical point. For  $t < 1$ , the chain is ordered: there are two ground states, one dominated by the configuration with by all spins up, the other dominated by the configuration with all spins down. In the height language, these correspond respectively to the configurations (121212...) and (323232...). For  $t > 1$ , the model is disordered. Thus  $t = 1$  is the well-known Ising critical point between the ordered and disordered phases. Excited states in the ordered phase contain defects, i.e. states which contain regions of both ground states locally. The equivalence of the Ising model to the dilute loop model with  $n = 2(\cos(\pi/3)) = 1$  was already discussed in the introduction. In the height language, the loops are domain walls separating regions of height 1 and height 3.

The two ground states in the  $p = 3$  case are symmetry-equivalent: the critical point is just the usual one where the discrete symmetry becomes no longer spontaneously broken. For  $p > 3$ , the different ground states are no longer all related by any obvious symmetry, but the fine tuning necessary to get to the integrable multi-critical point with Hamiltonian (14) makes them all degenerate.

To see this in more detail, consider the  $p = 4$  case, the ‘‘hard-square’’ model [11]. The hard-square tiles have diagonal length twice the lattice spacing, and are placed with their centers on the sites of a square lattice, with the rule that no two tiles can overlap. This then forbids tiles from being adjacent to each other. In the height language, this means that heights 1 and 4 correspond to the tiles, and 2 and 3 correspond to empty sites (on one sublattice the height is always even, on the other it

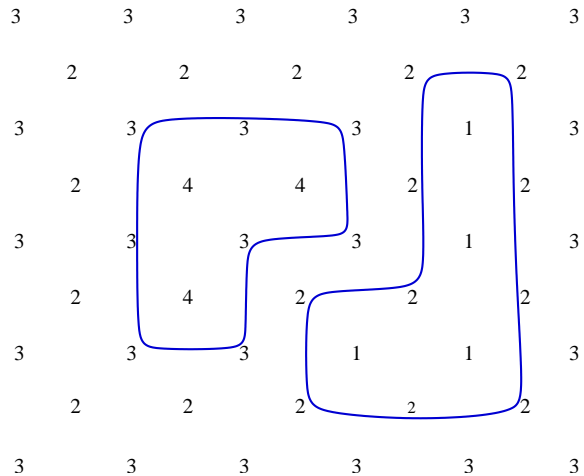


FIG. 9: A typical configuration in the RSOS height model with  $p = 4$ . The lines are the domain walls corresponding to dilute loops, drawn so that they do not cover the heights that they go through.

is always odd, and the Boltzmann weights are invariant under  $h \rightarrow p+1-h$ .) The restriction that  $|h_i - h_j| = 1$  for  $i$  next to  $j$  enforces the hard-square restriction. A typical configuration is displayed in figure 9. The Hamiltonian is easiest to write by treating the square tile as a hard-core boson created by  $d_i^\dagger$ . It is then [23]

$$\mathcal{H} = \sum_i \left[ -W (d_i + d_i^\dagger) (1 - n_{i-1})(1 - n_{i+1}) + Un_i + Vn_i n_{i+2} \right] \quad (15)$$

where  $n_i = d_i^\dagger d_i$  is the number operator at site  $i$ . The critical (14) corresponds to the values

$$W_c = \phi^{-1/2}, \quad V_c = -\phi^2, \quad U_c = 2 + 1/\phi^2 \quad (16)$$

where  $\phi = 2 \cos(\pi/5) = (1 + \sqrt{5})/2$  is the golden mean.

To understand the multiple ground states, it is useful to first take the limit where  $|U/W|$  and  $|V/W|$  are large, so that the off-diagonal term proportional to  $W$  can be neglected. For  $U > -V$  then the ground state is the state with no bosons, while for  $U < -V$  there are two ground states, each of which has a particle on every other site. In the latter regime, a  $\mathbf{Z}_2$  symmetry (translation by one site) is spontaneously broken. At  $U = -V$ , there is a first-order phase transition between the  $\mathbf{Z}_2$ -broken phase to an unbroken phase. In height language the two ground states in the  $\mathbf{Z}_2$ -broken phase are dominated by the states (...12121212...) and (...34343434...) respectively, while the single ground state in the unbroken phase (the empty state in the bosonic language) is dominated by (...32323232...). This first-order transition persists as  $W$  is included; doing perturbation theory gives the location of this transition at next order to be [23]

$$\frac{U}{V} = -1 + \frac{W^2}{V^2}, \quad (17)$$



Although the perturbative computation is only reliable to order  $(W/V)^2$ , it turns out that (17) is the exact first-order transition line for  $U > U_c$ . Along this line the two phases coexist – the hard-square model has three symmetry-equivalent ground states. When the couplings are tuned to the values in (16), this first-order line terminates in the tricritical point [11, 24].

This information about the ground states is sufficient to guess what the lowest-energy excitations are; in the next subsection III D I will justify these guesses using the corner transfer matrix. Excited states along this first-order transition line are defects, where two different ground states meet. For example, the state  $(\dots 32323232121212323232 \dots)$  has two defects, and energy order  $U$  higher than the ground state. Thus each of these defects has energy of order  $U/2$ . Such a defect occurs at site  $i$  any time  $|h_{i-1} - h_{i+1}| = 2$ . There are two kinds of fundamental defects, with the same energy. Denoting the three ground states as  $G_{12}$ ,  $G_{23}$  and  $G_{34}$ , where  $G_{ab} = (\dots abababab \dots)$ , one kind of fundamental defect separates  $G_{12}$  and  $G_{23}$ , while the other separates  $G_{23}$  and  $G_{34}$ . The former defect is located at the site where there is a height 2 between the heights 1 and 3, while the latter is located at the site where there is a height 3 between heights 2 and 4. A defect  $(\dots 1212343434 \dots)$  separating  $G_{12}$  from  $G_{34}$  has twice the energy as the fundamental defects, and is comprised of two fundamental defects.

These statements can be translated from the one-dimensional quantum Hamiltonian back to the two-dimensional hard-square model [24]. The three ground states of the Hamiltonian result in three different ways the free energy density can be minimized. One can easily check that at the critical point, the weight of the configuration with all heights 1 and 2 (which in a slight abuse of notation can be labeled  $G_{12}$ ) is larger than that of the configuration containing all heights 2 and 3 (the 2d analog of  $G_{23}$ ). On the first-order line, there are three different ways the free-energy density can be minimized. The reason is that there are more configurations “close” to  $G_{23}$  than there are to  $G_{12}$  or  $G_{34}$ , so the increased entropy will compensate for the increased energy. This is the cause as well of the shift of the first-order line in (17). With  $G_{23}$ , one can change any height 2 to height 4, and any height 3 to height 1, without violating the hard-square rule. With  $G_{12}$ , one can change any height 1 to height 3, but it is not possible to change any heights 2 to height 4 without violating the restriction, unless one also changes the four heights 1 around it. In the language of hard squares, there are more ways of adding a square to the empty configuration than there are of removing one from the full configuration, since in the latter the squares occupy only every other site. Thus the three ground states turn into the three minima of the free energy.

The partition function can therefore be rewritten as a sum over domain-wall configurations separating the free-energy minima. The excited states of the Hamilto-

nian become the domain walls in the 2d classical model, separating regions of  $\mathbf{Z}_2$  broken and unbroken symmetry. These domain walls are the world-lines of the one-dimensional defects, and their contribution to the free energy depends only on their length times some positive constant  $f_D$ . By the symmetry  $h \rightarrow p+1-h$ ,  $f_D$  must be the same for both kinds of domain wall. A non-vanishing  $f_D$  is the reason the transition is first-order: the tricritical point occurs when the couplings are tuned to make  $f_D \rightarrow 0$ . In this limit there is no free-energy penalty for creating a domain wall, and they proliferate.

It is finally possible to give the argument as to why the hard-square model is equivalent to a loop model, in the sense that they are described by the same field theories in the continuum limit. I have argued that the hard-square model along its first-order line can be thought effectively as having three free-energy minima. Domain walls separating regions of these minima have a free-energy weight per unit length. The domain walls form loops which do not touch: as noted above, domain walls separating  $G_{12}$  and  $G_{23}$  are located along sites with height 2, while domain walls separating regions  $G_{23}$  and  $G_{34}$  are located along sites with height 3. These domain walls are illustrated in figure 9. I emphasize that this picture involving free energies and domain walls is effective: these should be thought of as renormalized quantities.

Nevertheless, these results imply that along the first-order line, the partition function of the hard-square model can be written in the form

$$Z_{p=4} \approx \sum_{\mathcal{L}} w(\mathcal{L}) e^{-f_D L}. \quad (18)$$

$\mathcal{L}$  is a configuration of loops of total length  $L$  on the links of the dual square lattice, with the condition that they cannot touch. In this expansion, no distinction is made between the two different types of domain walls: the fact there are two types of loops can be taken into account in the weight  $w(\mathcal{L})$ . To do this, draw a loop configuration. The restrictions on heights mean that a loop separates a region of  $G_{23}$  from a region of either  $G_{12}$  or  $G_{34}$ . Since the energies of  $G_{34}$  and  $G_{12}$  are related by the  $\mathbf{Z}_2$  symmetry, we can then sum over these two possibilities. Half the regions inside the loops therefore must be  $G_{23}$ , while the other half can be either  $G_{12}$  or  $G_{34}$ . This results in a weight  $w(\mathcal{L}) = 2^{\mathcal{N}/2}$ , where  $\mathcal{N}$  is the total number of loops, so that the weight per loop is  $\sqrt{2}$ . This is the dilute  $O(n)$  loop model with  $n = \sqrt{2}$ . The (tri)critical point occurs at  $f_D = 0$  where there is no penalty for longer loops and they can proliferate.

The loop model therefore arises here indirectly, as opposed to the dilute Temperley-Lieb models, where the domain walls and hence the loops are manifest in the original lattice height configurations [20, 21]. All arguments give the same result: the conformal field theory with  $p = 4$  describes the critical point of the  $O(\sqrt{2})$  dilute loop model on the sphere.

### D. Dilute loops and the corner transfer matrix

In the preceding subsection III C I detailed an argument relating the RSOS model with  $p = 4$  to the  $O(\sqrt{2})$  loop model. The argument can be strengthened and generalized to arbitrary  $p$  by using the corner transfer matrix technique [11, 13]. The corner transfer matrix allows one to find the ground states in general, and also gives essential information about the defect energies.

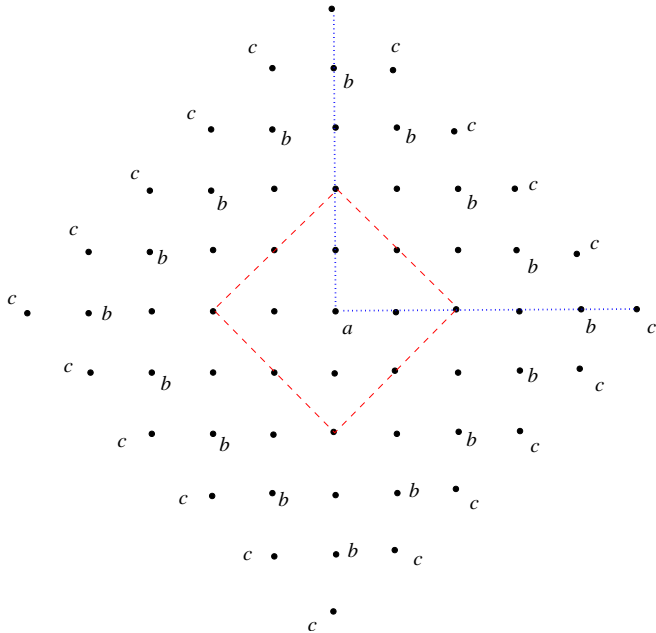


FIG. 10: The corner transfer matrix computes the partition function in one quadrant of the square. In the frozen limit, the spins are all the same along a given diagonal of each quadrant.

Consider a two-dimensional lattice model on a square lattice, as illustrated in figure 10. The corner transfer matrix acts on  $N$  sites along a line, taking them to  $N$  sites along a line *perpendicular* to the original line. The partition function for the full model is then built up from four corner transfer matrices.

The glory of the corner transfer matrix is that, as opposed to the usual transfer matrix, its eigenvalues can be determined exactly and explicitly if the model is integrable [11]. Its eigenvalues have special analyticity properties in one of the couplings ( $x$  here), which allows one to show that they must be independent of other couplings. In the hard-square model, the eigenvalues of the corner transfer matrix are the same along the entire first-order line. Therefore, they can be computed by going to the far “end” of this line, where in the Hamiltonian  $|U/w| = |V/w| \rightarrow \infty$ . In this limit, not only are the three states  $G_{12}$ ,  $G_{23}$  and  $G_{34}$  the exact ground states of the Hamiltonian, but every height configuration is an eigenstate. This limit is “frozen”, because in the two-dimensional lattice model all the heights along a diagonal are frozen to be the same. For example, in the northeast

and southwest quadrants of figure 10, the heights along each diagonal in the northwest/southeast direction must be the same. Moving away from the frozen limit, the eigenstates of the corner transfer matrix will change, but the eigenvalues, and hence the type of ground states, stay the same all along the first-order line. The same picture holds for all  $p$ : there is a first-order transition line going from a multicritical point to a frozen point.

From the corner transfer matrix eigenvalues one can compute the local height probabilities  $P(a|b, c)$ , defined as the probability that the height in the center will be height  $a$ , given that the heights around the edges of the square are  $b$  and  $c$ , as illustrated in figure 10. The  $N$  heights along a line starting at the center are labeled  $h_i$ , so that  $h_1 = a$ ,  $h_{N-1} = b$ , and  $h_N = c$ . Then [13]

$$P(a|b, c) = \mathcal{P}_a \sum_{\{h_2, h_3, \dots, h_{N-2}\}} q^{E(h_1, h_2, \dots, h_N)} \quad (19)$$

$$E(h_1, h_2, \dots, h_N) = \sum_{j=1}^{N-2} j |h_j - h_{j+2}| \quad (20)$$

where  $\mathcal{P}_a$  is a (known) factor independent of the heights other than  $h_1 = a$ , and  $q$  parametrizes the first-order line, so that  $q \rightarrow 0$  is the frozen limit and  $q \rightarrow 1$  is the multicritical point. The sum is over all allowed height configurations, and the contribution of each distinct configuration to this probability is obvious. The  $j$  in the expression for  $E$  arises because there are  $j$  sites along the  $j$ th diagonal, and in the frozen limit each site contributes equally to the eigenvalue.

The results found in the previous subsection III C using the Hamiltonian are therefore identical to those implied by the corner transfer matrix, and generalize to all  $p$ . Ground states in the frozen limit have  $E = 0$  in (20). These are states where the heights on every other site are the same, and it is natural to expect that the ground states all along the first-order line will be dominated by these configurations. Because of the restriction that  $|h_j - h_{j+1}| = 1$ , all states of the form  $G_{j, j+1} \equiv (\dots, j, j+1, j, j+1 \dots)$ . For the  $p$ th model, this means there are  $p - 1$  ground states. A defect at site  $j + 1$  occurs when  $|h_j - h_{j+2}| = 2$ ; such a defect runs all along the diagonal, and so has an energy of 2 per unit length in the units implied by (19,20). All defects have this energy per unit length, no matter which ground states they separate.

The translation of these results to the two-dimensional lattice model is essentially the same as for  $p = 4$  [16]. Each of the  $p - 1$  ground states  $G_{j, j+1}$  corresponds to a degenerate minimum of the free energy. Thus for  $q \rightarrow 0$  the partition function is dominated by regions of these minima, separated by domain walls which all have the same energy per unit length. For general  $p$ , as opposed to  $p = 3, 4$ , there is no symmetry forcing the domain walls to have the same energy, but rather it is a consequence of the fine tunings necessary to make the model integrable

and on the first-order transition line. As  $q \rightarrow 1$ , the multicritical point of interest is approached, and the energy per unit length of the domain walls goes to zero.

The restrictions on adjacent heights and on domain walls can be simply encoded in terms of *adjacency diagrams*. For heights, the diagram has a node for every allowed height, and two nodes are connected by an edge if the corresponding heights are allowed to be on adjacent sites. For ground states, the diagram has a node for every ground state, and two nodes are connected if a fundamental domain wall can separate the two ground states. The RSOS models discussed above have  $p - 1$  different ground states  $G_{12}, G_{23}, G_{34}, \dots$ . The fundamental domain walls separate successive ground states on this list: i.e. a region of  $G_{h,h+1}$  can only be adjacent to  $G_{h-1,h}$  and  $G_{h+1,h+2}$ . Thus in this case the adjacency diagrams for the heights and for the ground states look the same, except there are  $p$  nodes in the height diagram, and  $p - 1$  nodes in the ground-state diagram. For both types, the  $j$ th node is connected to the  $j + 1$  and  $j - 1$  nodes. The nodes of the ground-state diagram correspond to the edges of the height diagram; this remains true for the more general RSOS models discussed in the next section. The two diagrams for  $p = 5$  are displayed in figure 11.



FIG. 11: On the left, the adjacency diagram for the heights of the  $p = 5$  RSOS model; on the right, the adjacency diagram for the ground states of the same model.

By the same argument as for  $p = 4$ , these results make it likely that the  $p$ th minimal conformal field theory describes the continuum limit of the critical point of a loop model with partition function of the form (1,18):

$$Z_p \approx \sum_{\mathcal{L}} w(\mathcal{L}) e^{-fD L}. \quad (21)$$

with suitable boundary conditions. To obtain the topological weight  $w(\mathcal{L})$ , one must sum over all the height configurations consistent with a fixed loop configuration.

The simplest way to do this sum is to define the *adjacency matrix*  $\mathcal{A}$  for the ground states. This is the adjacency diagram in matrix form: each row and column of this matrix corresponds to a ground state, with the  $\mathcal{A}_{ab} = 1$  if the ground states labeled by  $a$  and  $b$  can be separated by a fundamental domain wall, and zero otherwise. For the RSOS models here, it is

$$\mathcal{A}_{rs} = \delta_{|r-s|,1} \quad (22)$$

for  $r, s = 1, \dots, p - 1$ . For example, for  $p = 5$  it is

$$\mathcal{A} = \begin{pmatrix} 0 & 1 & 0 & 0 \\ 1 & 0 & 1 & 0 \\ 0 & 1 & 0 & 1 \\ 0 & 0 & 1 & 0 \end{pmatrix}.$$

The topological weight  $w(\mathcal{L})$  is the number of height configurations possible for each loop configuration  $\mathcal{L}$ . This is easily written in terms of  $\mathcal{A}$ . Index each loop by  $j$ , such that it separates regions of ground states labeled by  $a(j)$  and  $b(j)$ . Then the number of allowed height configurations is

$$\sum_{a(j), b(j)} \prod_{j=1}^{\mathcal{N}} \mathcal{A}_{a(j), b(j)}$$

where the sum is over all ground states in each region. Thus adding another loop amounts to multiplying by  $\mathcal{A}$ . For a large number of non-intersecting loops  $\mathcal{N}$ , one therefore obtains

$$w(\mathcal{L}) \approx \lambda^{\mathcal{N}}$$

where  $\lambda$  is the largest eigenvalue of  $\mathcal{A}$ . For the adjacency matrix (22), this is

$$\lambda = 2 \cos\left(\frac{\pi}{p}\right).$$

Thus the RSOS models in this section indeed correspond in the continuum limit to the  $O(n)$  loop model with  $n = 2 \cos(\pi/p)$ . This agrees with the two earlier cases we derived:  $n = 1$  for the Ising model, and  $n = \sqrt{2}$  for the hard-square model.

A very nice corroboration of this picture comes from studying the scattering matrix of the 1+1 dimensional theory in the continuum limit of the first-order line [25]. In field-theory language, moving along the first-order line away from the multi-critical point corresponds to a perturbation by the relevant  $\Phi_{1,3}$  “energy” operator. This field theory is integrable like the underlying lattice model, so one finds the quasiparticles and their exact scattering matrix. These quasiparticles turn out to be kinks which are defects between  $p - 1$  ground states, exactly as we have seen. This identification of the worldlines of these kinks as the loops in the  $O(n)$  model with  $n = 2 \cos(\pi/p)$  was made long ago [26]. In fact, the correspondence is even closer: the scattering matrix itself can be expressed in terms of the Temperley-Lieb algebra [27]. Namely, there is a representation of  $I$  and  $e$  acting on the kinks, such that the two-particle scattering matrix for two particles of momentum  $p_1$  and  $p_2$  is

$$S(p_1, p_2) = f(p_1, p_2) (I + g(p_1, p_2)e) \quad (23)$$

where  $f$  and  $g$  are known functions. This correspondence between the loops and the world-lines of the kinks in the 1+1-dimensional description was exploited in [12] to discuss different loop models for the  $Q$ -state Potts models.

#### IV. NEW FULLY PACKED LOOP MODELS

In section III I gave a dilute and fully packed loop model associated with each RSOS height model of Andrews, Baxter and Forrester. The conformal minimal

models describe the critical points. In this and the next section the methods developed in the last section are used to find new loop models from more complicated RSOS height models. It is then natural to conjecture that the conformal field theories describing the critical points of these height models also describe critical points in these loop models.

### A. Fused RSOS models

The Boltzmann weights of the integrable lattice models studied here satisfy the Yang-Baxter equation. This very strong constraint allows many properties of the models to be computed exactly, like the spectrum of the corner transfer matrix discussed above.

Another thing the Yang-Baxter equation allows is a way to construct new integrable lattice models from known ones. This procedure is called *fusion*, and was invented in [28], and applied to height models in [29]. The fused models obtained from the RSOS models are labeled by an integer  $k$ , and each model within a series is labeled by the same integer  $p$  as before. Thanks to corner-transfer matrix computations [30], the conformal field theories describing the critical points of the fused RSOS models are known: they are the coset conformal field theories (A2), which have central charge (A3).

The states of the general integrable RSOS models are easiest to understand in terms of representations of a quantum-group algebra. A quantum-group algebra  $U_q(G)$  is a one-parameter deformation of a simple Lie algebra  $G$ . For generic values of the parameter  $q$ ,  $U_q(sl(2))$  has irreducible spin- $s$  representations corresponding to those of ordinary  $sl(2)$ , but when  $q$  is a root of unity such that  $q^{2(p+1)} = 1$ , only those with  $s < p/2$  are irreducible. The tensor product of the spin- $s$  representation with the spin-1/2 one is

$$(s) \otimes (1/2) = (s + 1/2) + (s - 1/2) \quad (24)$$

as long as all representations involved have  $s < p/2$ , so e.g.  $((p-1)/2) \otimes (1/2) = (p/2 - 1)$ . Except for this truncation, this is the same rule as for ordinary  $sl(2)$ .

Each allowed height  $h$  of a  $U_q(sl(2))$  RSOS model corresponds to the irreducible representation of spin  $(h-1)/2$ , so the heights run from  $1, \dots, p$ . Each fused model is labeled by an integer  $k$ . In the  $k$ th model, the height  $h_1$  is allowed to be adjacent to a height  $h_2$  if the corresponding representations of  $U_q(sl(2))$  have the tensor-product decomposition

$$\left(\frac{h_1 - 1}{2}\right) \otimes \left(\frac{k}{2}\right) = \left(\frac{h_2 - 1}{2}\right) + \dots \quad (25)$$

This can be interpreted physically by saying that the link variables of the fused models have spin  $k/2$ , with the original RSOS models discussed in section III A having  $k = 1$ . For  $k = 1$ , using the tensor product (24) indeed gives the adjacency diagram illustrated in figure 11. The tensor

products of higher-spin representations of  $U_q(sl(2))$  can be built up from (24). The fused RSOS models to be discussed in this section have  $k = 2$ , so the links have spin 1. The tensor product of a spin-1 representation can be found by using the fact that  $(1/2) \otimes (1/2) = (0) + (1)$ . Thus

$$(s) \otimes (1) = (s) \otimes (1/2) \otimes (1/2) - (s).$$

For  $s < p/2 - 1$ , the tensor product of  $(s)$  with  $(1)$  is thus the same as for ordinary  $sl(2)$ . The different rules come from the restriction that  $s < p/2$ . One has  $(p/2 - 1) \otimes (1) = (p/2 - 1) + (p/2 - 2)$ , while  $((p-1)/2) \otimes (1) = ((p-3)/2)$ . Note that  $((p-1)/2)$  does not appear on the right side of the latter, despite its being an allowed representation.

For the general model labeled by  $k$  and  $p$ , continuing in this fashion gives the constraints on nearest-neighbor heights  $h_i$  and  $h_j$  to be [29]

$$\begin{aligned} h_i &= 1, 2 \dots p \\ h_i - h_j &= -k, -k + 2, \dots, k \\ k + 1 &< h_i + h_j < 2p - k + 1 \end{aligned} \quad (26)$$

These rules are symmetric under the interchange  $h \rightarrow p + 1 - h$ . The Boltzmann weights for  $k = 1$  satisfy this symmetry as well, so those for higher  $k$  found by fusion satisfy this as well. For  $k$  even, all heights in a given configuration must be even or odd. It then is consistent to restrict them all to be even, because one obtains the same field theory for even or odd.

### B. Fully packed loop models for $k = 2$

I show here how to derive fully packed loop models for the  $k = 2$  fused RSOS models. This is done in a similar fashion as for the  $k = 1$  case, by rewriting the transfer matrix in terms of the generators of an algebra, and then finding a graphical representation generalizing that of the Temperley-Lieb algebra.

The transfer matrix for all  $k$  can be written in the form (9). For  $k = 2$ , the weights for each plaquette are then

$$\mathcal{T}_i = I_i + xX_i + yE_i \quad (27)$$

where  $x$  and  $y$  are parameters related by

$$\begin{aligned} y &= x + Q \frac{x^2}{1-x}, \\ \sqrt{Q} &= q + q^{-1} = 2 \cos(\pi/(p+1)). \end{aligned}$$

The model is isotropic when  $x = 1/(\sqrt{Q} + 1)$  and  $y = 1$ . The Hamiltonian

$$H = - \sum_i (X_i + E_i) \quad (28)$$

follows from the  $x \rightarrow 0$  limit. The representation of  $X_i$  and  $E_i$  in terms of the heights is given in appendix C.

There is one important difference between  $X_i$  and the Temperley-Lieb generators:  $X_i$  can be non-zero when both pairs of heights across a plaquette are different (i.e.  $h_i \neq h'_i$  and  $h_{i-1} \neq h_{i+1}$ ). This has important consequences for both the dilute and fully packed loop models.

The lattice model with weights (27) is integrable when the  $X_i$  and  $E_i$  satisfy an algebra known as the  $SO(3)$  Birman-Murakami-Wenzl (BMW) algebra [31]. This algebra is best thought of as the spin-1 generalization of the Temperley-Lieb algebra. In fact, any representation of the Temperley-Lieb algebra yields one of the  $SO(3)$  BMW algebra [32]; expressions for  $X_i$  and  $E_i$  in terms of the  $e_i$  are given in appendix C. The algebraic relations of the  $X_i$  and  $E_i$  can be found in [32], and are given in appendix C.

As with lattice models based on the Temperley-Lieb algebra, many of the properties of the models with Boltzmann weights (27) are independent of the representation of the  $X_i$  and  $E_i$ . The most illuminating representation of these generators is a graphical one. To find this, it is useful to study first another representation of the same algebra [32, 33].

This representation arises in the  $Q$ -state Potts model with infinitely-strong antiferromagnetic nearest-neighbor interactions, and ferromagnetic next-nearest-neighbor interactions. A “spin”  $s_i$ , taking the integer values  $s_i = 1 \dots Q$ , is placed at each site  $i$  of the square lattice. The restriction on nearest-neighbor spins is simpler than that of the height models: adjacent spins must be different. If all configurations were weighted equally, this would be the antiferromagnetic  $Q$ -state Potts model at zero temperature. However, at the critical point of interest, there are ferromagnetic next-nearest-neighbor interactions. Labeling the spins around a plaquette as  $s_{i-1}$ ,  $s_i$ ,  $s_{i+1}$  and  $s'_i$ , in the same fashion as the heights in figure 6, the restriction on nearest neighbors means that

$$\Gamma_i \equiv \delta_{s_{i-1}s_i} \delta_{s_i s_{i+1}} \delta_{s_{i+1}s'_i} = 1$$

for each plaquette. The transfer matrix is then given by (27), with

$$\begin{aligned} I_i &= \Gamma_i \delta_{s_i s'_i} \\ X_i &= \Gamma_i \\ E_i &= \Gamma_i \delta_{s_{i-1} s_{i+1}} \end{aligned} \quad (29)$$

It is easy to check that these satisfy the  $SO(3)$  BMW algebra with  $Q = (q + q^{-1})^2$  [32]. For  $Q \leq 4$  there is a critical point described by a conformal field theory with  $c = 1$  for  $Q = 3$  and  $c = 3/2$  for  $Q = 4$ . Using (29) in the Hamiltonian (28) makes it clear that the next-nearest-neighbor interaction wants to make spins the same, so this critical point presumably separates an ordered phase from a disordered one.

A graphical representation of  $I$ ,  $E$  and  $X$  in (29) is presented in figure 12. The lines represent domain walls between different spins; any spins not separated by a domain wall must be the same. The  $X$  generator has regions

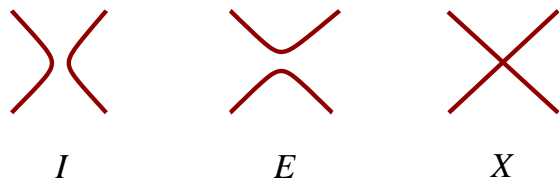


FIG. 12: The graphical representation of the  $SO(3)$  BMW algebra

touching only at a point; these may (but need not) have the same spin.

A fully packed loop model is obtained in the same fashion as the Temperley-Lieb case. The partition function is expanded out in powers of  $x$  and  $y$ . Each term corresponds to a loop configuration after the heights are summed over. The generators  $I$  and  $E$  are 90-degree rotations of each other, so a rotationally-invariant model is obtained by taking  $y = 1$  and  $x = 1/(\sqrt{Q} + 1)^{-1}$  in (27). This yields a loop model with a typical configuration illustrated in figure 4. The loops here have a very important difference with the self- and mutually-avoiding loops of the  $O(n)$  loop model: because of the  $X$  vertex, the loops can touch. (Thus properly speaking, they shouldn’t even be called loops, but rather graphs with quadrivalent vertices.)

Since the  $k = 2$  RSOS height models are based on a different representation of the same  $SO(3)$  BMW algebra, these have the same partition function as the loop models when  $\sqrt{Q} = q + q^{-1} = 2 \cos(\pi/(p+1))$  for  $p$  integer. Therefore the loop models at these values of  $p$  also have critical points with the same conformal field theory description, the superconformal minimal models. The graphical representation is valid for all  $Q$ , not just the  $Q$  integer where (29) applies, or for  $Q = 4 \cos^2(\pi/(p+1))$  with  $p$  integer for the height models. It is likely that these loop models have a critical point for all  $Q \leq 4$ , although its field-theory description will only be unitary for  $p$  integer.

The topological weight can be worked out using the BMW algebra. However, it is much simpler to find it by using the representation (29) valid for integer  $Q$ . The lines in the graphical representation correspond to domain walls for the spins  $s_i$ . This constrains spins in regions separated by domain walls to be different (if two regions meet only at a point, the corresponding spins are still permitted to be the same). Each allowed spin configuration then receives the same weight, so the topological weight per loop configuration is given by the number of different spin configurations. This is simply the number of ways of coloring the regions with  $Q$  colors, subject to the constraint that adjacent regions have different colors. This is simply  $\chi_Q$ , as defined in section II. This argument holds true for any positive integer  $Q$ . This can be generalized uniquely to arbitrary  $Q$  by recognizing that  $\chi_Q$  for a given dual graph satisfies the recursion relation (6), and thus is a polynomial in  $Q$ . Thus the sum over



heights for any  $Q$  yields  $\chi_Q$ . To get the full topological weight, note that every time an  $X_i$  appears in the expansion of the partition function, it comes with a weight  $x = 1/(\sqrt{Q} + 1)$ , as detailed after equation (27). The number of  $X$  vertices  $\mathcal{N}_X$  is a topological invariant. The topological weight is therefore that given in (7), namely

$$w(\mathcal{L}) = \chi_Q(\mathcal{L})(\sqrt{Q} + 1)^{-\mathcal{N}_X}.$$

This completes the mapping of the  $k = 2$  RSOS height models onto the loop model described in section II. However, this fully packed loop model is not the only one in this universality class. As described in appendix C, the  $SO(3)$  BMW algebra can be written in terms of the Temperley-Lieb generators. In this representation, there are two lines on every link, with a projection operator  $\mathcal{P}_i$  ensure that the two are in the spin-1 representation of  $U_q(sl(2))$ . Therefore, the graphical representation in figure 7 can be used with (C1) to give a fully packed loop model on the  $CuO_2$  lattice. The  $CuO_2$  lattice is formed by taking a square lattice (the coppers), and adding an extra site on each link (the oxygens). At every copper site, one gets  $I$ ,  $X$ , or  $E$  as above. However, instead of using the above graphical representation with an intersection for  $X$ , one writes them instead in terms of  $I$  and  $e$  using (C1), and uses figure 7 to represent them graphically (illustrations can be found in [32]). The projectors on the links (the oxygen sites) are expanded in terms of  $I$  and  $e$  as well, by using  $\mathcal{P}_i = 1 - e_i/(q + q^{-1})$ . This means that on the oxygen sites as well. This yields a somewhat strange but well-defined fully packed loop model on the  $CuO_2$  lattice, which has a critical point described by the superconformal minimal models. This construction can readily be generalized to larger  $k$  integer as well.

## V. NEW DILUTE LOOP MODELS

In this section I give a dilute-loop description of the  $k = 2$  height models and superconformal minimal models. The methods are similar to those used in sections III C and III D for the  $k = 1$  height models and the conformal minimal models. As opposed to the precise results for the fully packed loop models, the mapping for dilute loops is indirect, and thus is just a conjecture, not a proof.

The corner transfer matrix results for the fused RSOS models have long been known [30]. The results of interest are along an integrable line of couplings, known as ‘‘Regime III’’ in the literature. Like for the hard-square and  $k = 1$  RSOS models, along this line, the Hamiltonian (28) has degenerate ground states. This is apparent from the computation of the local height probabilities from the corner transfer matrix. The formula is identical to the earlier case; the only distinction is that the restrictions on the heights are different. Namely, the local height probability is still given by (19), where  $q$  parametrizes the integrable line of couplings, with  $q \rightarrow 0$  the frozen limit and  $q \rightarrow 1$  is the multicritical point.

### A. Dilute loop models for $k = 2$

For  $k = 2$ , the heights are even integers  $h_i \leq p$ , and  $h_i$  and  $h_j$  on adjacent sites obey  $h_i - h_j = 0, \pm 2$  and  $2 < h_i + h_j < 2p$ . It is convenient to distinguish between heights on the two sublattices of the square lattice, each sublattice comprised of every other site. Denoting heights on one sublattice without a bar, and one with a bar, the adjacency diagrams for the  $k = 2$  height models with  $p = 6$  and  $p = 7$  are given in figure 13. Unbarred heights are always adjacent to barred heights, and vice versa.

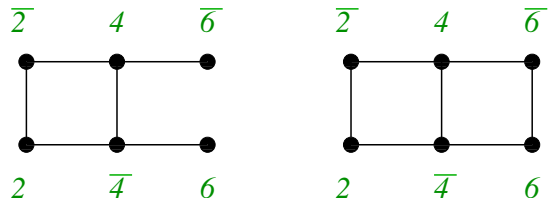


FIG. 13: the adjacency diagrams for the heights of the fused RSOS model with  $k = 2$ ,  $p = 6$  (left) and  $k = 2$ ,  $p = 7$  (right).

The energy  $E$  in (20) is minimized when the heights on every other site are the same. This is an exact ground state of the model in the frozen limit. As argued in section III D, each configuration with this property should correspond to a ground state of the Hamiltonian all along the integrable line, including at the multicritical point, where  $H$  is given in (28). These ground states are therefore of the form  $G_{h,\bar{h}} = (\dots h\bar{h}h\bar{h}\dots)$  and  $G_{h,\overline{h\pm 2}} = (\dots h, \overline{h\pm 2}, h, \overline{h\pm 2}, \dots)$ . As before, each ground state corresponds to an edge on the height adjacency diagram. Excited states are defects between ground states. For the  $k = 1$  case, a defect at site  $i$  means  $h_{i+1} - h_{i-1} = \pm 2$ . Here, a defect can have  $h_{i+1} - h_{i-1} = \pm 2$  or  $\pm 4$ . However, for the latter defect,  $E$  in (20) is twice as large. It is therefore natural to assume that  $\pm 4$  defects can be treated as two of the  $\pm 2$  defects. (Thus one can have a ‘‘double defect’’ on one plaquette.) Thus fundamental defects are only those where  $h_{i-1} - h_{i+1} = \pm 2$ , so the adjacency diagram for ground states looks like those illustrated in figure 14. Another way of making the distinction between fundamental and composite defects is that a fundamental defect occurs between  $G_{h_1\bar{j}_1}$  and  $G_{h_2\bar{j}_2}$  if either  $h_1 = h_2$  or  $j_1 = j_2$ .

The ground states and fundamental defects are easiest to list in terms of new labels. Relabel ground states of the form  $G_{h,\bar{h}}$  as  $\mathcal{G}_{h-1}^2$ , those of the form  $G_{h,\overline{h+2}}$  as  $\mathcal{G}_h^1$ , and those of the form  $G_{h+2,\bar{h}}$  as  $\mathcal{G}_h^3$ . The different ground states  $\mathcal{G}_s^r$  then have  $r = 1 \dots 3$ , and  $s = 1 \dots p - 2$  with  $r + s$  odd. The fundamental defects then separate the ground states  $\mathcal{G}_{s_1}^{r_1}$  and  $\mathcal{G}_{s_2}^{r_2}$  if  $r_1 = r_2 \pm 1$  and  $s_1 = s_2 \pm 1$ . Note that with this relabeling, the constraints on  $r$  and  $s$  are independent of each other. Moreover, the constraints on  $r$  and  $s$  individually are exactly the same as for the ground states of the  $k = 1$  height models. This means

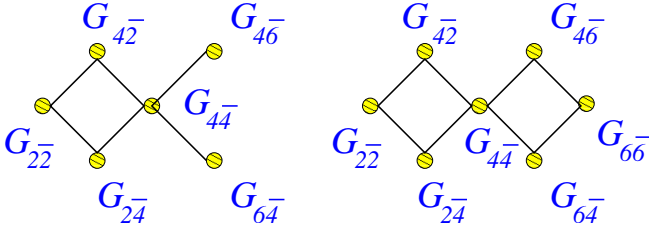


FIG. 14: The ground-state adjacency diagrams for  $k = 2, p = 6$  (left), and  $k = 2, p = 7$  (right).

that the ground-state adjacency matrix for the  $k = 2$  models can be written as the tensor product

$$\mathcal{A}^{2,p} = \mathcal{A}^{1,4} \otimes \mathcal{A}^{1,p-1} \quad (30)$$

where we denote the adjacency matrices for general  $k$  and  $p$  by  $\mathcal{A}^{k,p}$ . The adjacency matrix for the heights does *not* obey such a simple decomposition: this is only a property of the ground states and fundamental defects.

As with the  $k = 1$  case, the world lines of the fundamental defects are interpreted in the two-dimensional lattice model as domain walls between free-energy minima. These domain walls form the loops. Domain walls in these RSOS models occur when heights *across* a square plaquette are different. These domain walls are drawn on the *diagonals* of the original lattice, as seen in the (non-intersecting) loops of figure 9. (In the fully packed loop models, the links are drawn on the links of the dual lattice.) Each link of the original lattice corresponds to a ground state, so the domain walls separate links with different ground states.

To complete the argument, the topological weight  $w(\mathcal{L})$  of each loop configuration must be found. The simplest possibility, realized for  $k = 1$ , is that is that these domain walls never cross, so that the loops self-avoid and mutually avoid. Summing over the heights in the model then gives the topological weight of the  $O(n)$  loop model:  $w = n^{\mathcal{N}}$ , where  $\mathcal{N}$  is the number of loops. For several reasons, such a  $w$  cannot be correct for  $k > 1$ .

First of all, domain walls do cross for  $k > 1$ . This happens when all four ground states around a link are different. In the  $k = 2$  model, the domain walls cross when the heights around a plaquette are of the forms

$$\begin{array}{cc} \begin{array}{c} h+2 \\ \overline{h} \quad \overline{h+2} \\ h \end{array} & \begin{array}{c} h \\ \overline{h} \quad \overline{h+2} \\ h+2 \end{array} \end{array} \quad (31)$$

The four different ground states on these two plaquettes are  $G_{h,\overline{h}}$ ,  $G_{h+2,\overline{h}}$ ,  $G_{h+2,\overline{h+2}}$  and  $G_{h,\overline{h+2}}$ . These have a non-zero Boltzmann weight coming from  $X_i$ , as given in appendix C. Configurations like these cannot occur in the  $k = 1$  model, where  $I_i$  requires that the top and bottom heights be the same, while  $e_i$  requires that the left and right be the same.

Even if one were to assume that such crossings are irrelevant, the value of  $n$  obtained is still inconsistent. Namely, if crossings are ignored, one obtains the dilute  $O(n)$  loop models as with  $k = 1$ . The arguments of section III D give the weight  $n$  per loop to be the largest eigenvalue of  $\mathcal{A}$ . This is easy to find from (30): it is simply the product of the largest eigenvalues of  $\mathcal{A}^{1,4}$  and  $\mathcal{A}^{1,p-1}$ , which are  $2 \cos(\pi/4) = \sqrt{2}$  and  $2 \cos(\pi/(p-1))$  respectively. This would yield  $n = 2\sqrt{2} \cos(\pi/(p-1))$ . Although this is the precise value of  $n$  implied by the SLE results [9], the loop model cannot be the  $O(n)$  model. The weight per loop has  $n > 2$  (e.g.  $n = 2\sqrt{2}$  for the  $SU(2)_2$  WZW model) in general, and the  $O(n)$  model in this regime does not have a critical point. Since the underlying lattice model is critical, a non-critical loop model obviously cannot be an equivalent description. The fact that domain walls can cross or touch must affect the continuum behavior of the loop model.

The fact that the weight of non-crossing loops is the same as the SLE results is quite encouraging. The task is then to use the Boltzmann weights of the height model to understand how to treat the crossings. The fully packed loops do intersect, and affect the topological weight via the chromatic polynomial. The dilute loops behave differently. The decomposition (30) suggests that for  $k > 1$  the domain walls should not be treated as a single lines, but instead split into *two* lines, *each* of which behaves as a  $k = 1$  model.

The key to defining a topological weight is the relabeling of the ground states as  $\mathcal{G}_r^s$  as described above. In this relabeling, the  $r$  and  $s$  labels behave independently, as far as the adjacency restrictions on the ground states are concerned. Since the domain walls are between the ground states, this means the domain walls in the  $r$  and  $s$  labels can be treated independently. Thus the domain walls can be split into a “solid” wall and a “dashed” wall, as illustrated in figure 2. Away from where the domain walls meet, this splitting is unimportant, and the solid and dashed lines are attached. However, at a domain-wall crossing there are now *four* ways of resolving the lines so that lines of the same type do not cross. These are illustrated in figure 15. The dashed line is a domain

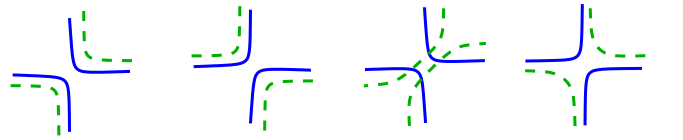


FIG. 15: The four ways of resolving a domain-wall crossing with doubled lines

wall in the 1, 4 theory (the  $r$  index in  $\mathcal{G}_r^s$ ), while the solid line corresponds to a domain wall in the 1,  $p-1$  model (the  $s$  index in  $\mathcal{G}_s^r$ ).

Note that dashed lines never cross or touch each other, and likewise for solid, but that the dashed and solid can cross one another. Thus a loop configuration consists of dashed and solid loops which are sewn together, except

when two loops meet on one plaquette. At each domain-wall crossing, one of the four possibilities in figure 15 must occur. A typical loop configuration is illustrated in figure 2. Since the restrictions on the  $r$  and  $s$  labels are completely independent, it is consistent to treat the dashed and solid domain walls independently.

All the configurations in the height model can therefore be realized in terms of a pair of  $k = 1$  domain walls. The last two domain-wall configurations in figure 15 are necessary to realize configurations like (31) that occur for  $k > 1$ . This follows from rewriting the ground states around the plaquette in terms of  $\mathcal{G}_s^r$ . For example,  $G_{h,\bar{h}} = \mathcal{G}_{h-1}^2$  and  $G_{h+2,\overline{h+2}} = \mathcal{G}_{h+1}^2$ . Therefore they have the same  $r$  value and are not separated by any dashed lines. Likewise  $G_{h+2,\bar{h}} = \mathcal{G}_h^3$  and  $G_{h,\overline{h+2}} = \mathcal{G}_h^1$  so these have the same  $s$  value and are not separated by any solid lines.

This picture is in remarkable accord with the field-theory results for the ( $k = 2$ ) superconformal minimal models perturbed along the integrable line of interest. The particles in the field theory have the same labels as the defects, so the particle world-lines can again be identified with the domain walls. Moreover, the scattering matrix  $S^{2,p}$  is a product of  $k = 1$  scattering matrices [34], just like the ground-state adjacency matrices. It is

$$S^{2,p} = S^{1,4} \otimes S^{1,p-1}. \quad (32)$$

Plugging the  $k = 1$  scattering matrices from (23) into (32) shows that  $S^{2,p}$  is a sum of four terms, involving  $I \otimes I$ ,  $e \otimes I$ ,  $I \otimes e$ , and  $e \otimes e$ . Recalling the graphical representation of  $I$  and  $e$  in figure 7 gives precisely the four possibilities in figure 15 for the particle world-lines.

It is now clear how to build a topological weight for these dilute loops. The dashed and solid lines each form closed loops. The sum over heights can be done independently for the  $r$  and  $s$  labels for each ground state. The weight per dashed loop is then simply the largest eigenvalue of the  $\mathcal{A}^{1,4}$  adjacency matrix, which is  $\sqrt{2}$ . The weight per solid loop is the largest eigenvalue of  $\mathcal{A}^{1,p-1}$ , which is  $2 \cos(\pi/(p-1))$ . When the numbers of dashed and solid loops are  $\mathcal{M}$  and  $\mathcal{N}$  respectively, the topological weight is

$$w(\mathcal{L}) = \sqrt{2}^{\mathcal{M}} \left( 2 \cos \left( \frac{\pi}{p-1} \right) \right)^{\mathcal{N}} b^{\mathcal{C}}. \quad (33)$$

The topological invariant  $\mathcal{C}$  is the number of times the (original) domain walls cross, i.e. the number of plaquettes which have one of the configurations in figure 15 at their center. The piece involving the parameter  $b$  is analogous to the last piece of the fully packed weight (7). The arguments here are not refined enough to determine the value of  $b$ , or whether changing it results in a relevant or irrelevant perturbation of the critical point.

## B. Arbitrary $k$

The ground states for general  $k$  are quite analogous to those for  $k = 1$  and  $k = 2$ . The expression (19,20) for

the local height probabilities still holds, so the minimum of  $E$  occurs when the heights on every other site are the same. Thus each ground state can be labeled by two heights  $h_i$  and  $h_j$ , which must satisfy the constraints for nearest-neighbor heights in (26).

For general  $k$  and  $p$  integer, the adjacency matrix decomposes into tensor products of  $k = 1$  adjacency matrix. This follows by relabeling the ground states  $G_{h_1,h_2}$  into the form  $\mathcal{G}_s^r$  via

$$\begin{aligned} r &= \frac{h_1 - h_2 + k + 2}{2}, \\ s &= \frac{h_1 + h_2 - k}{2}. \end{aligned}$$

The constraints in (26) in terms of  $r$  and  $s$  are therefore quite simply  $r = 1, 2, \dots, k+1$  and  $s = 1, 2, \dots, p-k$ .

A fundamental defect needs to have energy  $E = 2$  in (20). This only occurs if the two ground states have one of their height labels in common, and one different. Namely, a fundamental defect separates the ground state  $G_{h_1,h_2}$  from the ground states  $G_{h_1,h_2 \pm 2}$  and  $G_{h_1 \pm 2,h_2}$ . In terms of  $r$  and  $s$  labels, this means that a fundamental defect separates  $\mathcal{G}_s^r$  from the states  $\mathcal{G}_{s \pm 1}^{r \pm 1}$  and  $\mathcal{G}_{s \pm 1}^{r-1}$ . Thus the restrictions on  $r$  and  $s$  are independent of each other, and the adjacency matrix for the ground states for general  $k$  and  $p$  is simply

$$\mathcal{A}^{k,p} = \mathcal{A}^{1,k+2} \otimes \mathcal{A}^{1,p-k+1} \quad (34)$$

This is in harmony with the scattering matrix for the quasiparticles in the field theory describing the integrable line, which is [35]

$$S^{k,p} = S^{1,k+2} \otimes S^{1,p-k+1}. \quad (35)$$

This also is in harmony with the Coulomb-gas approach to these conformal field theories, which gives their partition functions as sums of products of minimal-model ones [36].

The configurations in the dilute loop model for general  $k$  are therefore the same as for  $k = 2$  model. The defect world-lines become “double” domain walls in the two-dimensional picture. Crossings are resolved in the four ways in figure (15), so the typical configuration displayed in figure 2 still is applicable here. The weight for the dashed loops for general  $k$  is now the largest eigenvalue of  $\mathcal{A}^{1,k+2}$ , which is  $2 \cos(\pi/(k+2))$ . This yields the topological weights given in (3,4).

## VI. FURTHER DIRECTIONS

In this paper I have shown how to turn lattice models into loop models. Dense loop models are found directly by exploiting the algebraic structure of the transfer matrix, while dilute loops are the domain walls found more indirectly using the corner transfer matrix and the scattering matrix. Since these lattice models have critical

points described by known coset conformal field theories, this means that the loop models have these same critical points as well.

It would be interesting to show directly that the dilute loop models have these critical points. One way of doing so would be to study the “dilute BMW models” [37]. These lattice models generalize the dilute Temperley-Lieb models [20, 21] discussed above to allow a more general algebra. The domain walls for the dilute  $SO(4)$  BMW model are exactly the same doubled domain walls as in the dilute loop model discussed here (because the algebra  $SO(4) = SU(2) \times SU(2)$ ). The corner transfer matrix computation for these models has not yet been done, so it is not yet known if these models have the critical points described in this paper.

It would also of course be interesting to generalize these results to other loop models and conformal field theories. Another loop model with a critical point described by the conformal minimal models was discussed at length in [12]. This dilute loop model can be derived from the Potts lattice model from both the domain-wall and the algebraic approach (using projection operators instead of  $I, X$  and  $E$ ), but the heuristic approach used there is more suggestive. This is the scattering matrix approach used above, where the world lines of the particles in the field theory are identified with the loops. As mentioned briefly in [12], the scattering matrix approach suggests that the dilute version of the fully packed  $k = 2$  model discussed above will have critical points described by parafermion conformal field theories. This could be tested directly by studying the  $SO(3)$  dilute BMW model of [37].

Many integrable lattice models and scattering matrices are known, and it likely that the methods described here could be applied to them. Finding more examples would be of great interest in both the areas mentioned in the introduction: SLE and non-abelian statistics. Much is known about the relations between conformal field theory, non-abelian statistics, topology and geometry in the simplest cases. Hopefully the generalizations described here will be of use in deepening this knowledge.

**Acknowledgments** I am grateful to John Cardy, Eduardo Fradkin, Michael Freedman, Ilya Gruzberg, Andreas Ludwig, Nick Read, Kevin Walker, and Paul Wiegmann for many interesting conversations on loop models and related topics. This research has been supported by the NSF under grant DMR-0412956.

## APPENDIX A: A BRIEF REVIEW OF THE CONFORMAL FIELD THEORIES

Field theories describing rotationally-symmetric two-dimensional classical critical points are invariant under conformal transformations of two dimensional space. Conformal symmetry in two dimensions is very powerful, because it has an infinite number of generators: representations of the corresponding symmetry algebra (called

the Virasoro algebra) are infinite-dimensional. *Minimal models* are conformal field theories which have a finite number of highest-weight states under the conformal symmetry [4]. These are among the models for which SLE is applicable. The minimal models have been classified, and all the critical exponents are known [4, 38]. Many (and in principle, all) of the correlation functions can be explicitly computed. A convenient way of labeling conformal field theories is in terms of a number  $c$  called the *central charge*. Unitary minimal models have central charge

$$c = 1 - \frac{6}{p(p+1)}. \quad (\text{A1})$$

where  $p$  is an integer obeying  $p \geq 3$ . These are the only unitary conformal field theories with  $c < 1$  [38]. Any theory with  $c \geq 1$  has an infinite number of highest-weight states [39].

To study more general conformal field theories, it is useful to extend the Virasoro algebra by some other generators. One well-studied way of doing so is to extend the symmetry by a simple Lie algebra  $G$ . These conformal field theories are called Wess-Zumino-Witten (WZW) models [40], and the extended symmetry algebra is called a Kac-Moody algebra. Like with the minimal models, all critical exponents are known, and correlators can be computed explicitly [41]. Each unitary WZW model  $G_k$  is labeled by the algebra  $G$  and an integer  $k \geq 1$ , called the level.

Minimal models can be constructed from WZW models by using the *coset* construction [42]. A  $G/H$  coset conformal field theory is defined with energy-momentum tensor  $T_{G/H} = T_G - T_H$ , where  $T_G$  and  $T_H$  are the energy-momentum tensors of the  $G$  and  $H$  WZW models. This allows many of the properties (e.g. the critical exponents) of the coset models to be computed by using results from the WZW models. The coset models of interest here are

$$\frac{SU(2)_k \times SU(2)_{p-k-1}}{SU(2)_{p-1}} \quad (\text{A2})$$

with  $p > k + 1$ . They have central charge

$$c = \frac{3k}{k+2} \left( 1 - \frac{2(k+2)}{(p+1)(p-k+1)} \right). \quad (\text{A3})$$

When  $k = 1$ , these are the minimal models. The models with  $k = 2$  are usually known as the  $\mathcal{N} = (1, 1)$  superconformal minimal models, because they have an extended symmetry algebra including supersymmetry. Note that the simplest superconformal minimal model (with  $k = 2, p = 4$ ) is identical to the second conformal minimal model (with  $k = 1, p = 4$ ). As  $p \rightarrow \infty$  for fixed  $k$ , one obtains simply the  $SU(2)_k$  WZW model. The Coulomb-gas formulation of these coset models was developed in [36].

In the loop models discussed below,  $p$  becomes a continuous parameter. The conformal field theories describing loop models for  $p$  non-integer generally are expected

to be non-unitary and not rational. Exact computations are still possible by using the Coulomb-gas technique within conformal field theory, and (for  $c \leq 1$ ) SLE.

## APPENDIX B: LOOPS ON THE SPHERE

All the results of this paper apply when two-dimensional space is topologically a sphere. In this appendix I show how to implement these boundary conditions with the transfer matrix written in terms of Temperley-Lieb generators, and show that the partition functions in this situation are independent of representation of this algebra.

In a loop model, space is topologically a sphere when no loops end on the boundary. To implement these boundary conditions in the transfer-matrix formulation of the height model, define the operator

$$\mathcal{B} = (q + q^{-1})^N e_1 e_3 \dots e_{2N-1},$$

which acts on a zig-zag row of heights as illustrated in figure 6, acting on a set of heights  $h_0, h_1, \dots, h_{2N}$ .  $\mathcal{B}$  is normalized so that  $\mathcal{B}^2 = \mathcal{B}$ . Then the partition function for  $M + 1$  zig-zag rows is

$$Z_{\text{height}} = (\mathcal{B} T^M \mathcal{B})_{\{a\}\{a\}}$$

where  $\{a\}\{a\}$  means the matrix element which has all the heights in the first and last rows fixed to be  $a, a + 1, a, a + 1, \dots$ . The fact that  $T$  involves only  $I_0$  and  $I_{2N}$  for the left- and right-most columns means that all the heights along the sides are fixed to the same values.

To relate this definition of  $Z$  with that coming from the loops, expand  $T$  in terms of the Temperley-Lieb generators, as done for the fully packed loop models. Each of the resulting terms corresponds to a loop configuration  $\mathcal{L}$ , and consists of many  $e_i$  sandwiched in between the  $\mathcal{B}$ s. Consider one of these terms, which gets weight  $A(\mathcal{L})$  in the loop model, and  $A_{\{a\}\{a\}}$  in the height model. Then using the algebra (13), I show here that

$$A(\mathcal{L}) \mathcal{B}_{\{a\}\{a\}} = A_{\{a\}\{a\}}. \quad (\text{B1})$$

When computing  $A(\mathcal{L})$  the  $e_i$  in  $\mathcal{B}$  are drawn with only one loop: the piece that goes ‘‘off the edge’’ is ignored. The relation (B1) shows that up to an overall constant, the partition functions are the same:

$$Z_{\text{loop}} = \mathcal{B}_{\{a\}\{a\}} Z_{\text{height}} \quad (\text{B2})$$

Let  $j$  be an integer. Because  $(e_i)^2 = (q + q^{-1})e_i$  and all  $e_{2j-1}$  commute with each other,

$$e_{2j-1} \mathcal{B} = \mathcal{B} e_{2j-1} = (q + q^{-1}) \mathcal{B}.$$

Thus any time an  $e_{2j-1}$  is next to  $\mathcal{B}$ , it can be removed, leaving an overall factor  $q + q^{-1}$ . Now consider an  $e_2$  somewhere in the middle. All one needs to do to get rid of it is to get the  $e_1$ s from the  $\mathcal{B}$ s next to the  $e_2$ , and

then use  $e_1 e_2 e_1 = e_1$ . Since  $e_1$  commutes with everything other than  $e_2$ , the only obstruction to doing this is the product is of the form

$$e_1 e_2 \dots e_3 \dots e_2 e_1.$$

where  $e_1$  does not appear in the dots. Since there are no  $e_1$ s in the dots,  $e_2$  can be commuted through the dots and  $e_2 e_3 e_2 = e_2$  used, unless there is an  $e_4$  within the dots, i.e. the product is of the form

$$e_1 e_2 e_3 \dots e_4 \dots e_3 e_2 e_1.$$

The offending  $e_4$  can then be eliminated using the  $e_3$ s unless there is an  $e_5$  which interferes. Thus either the offending ones can be eliminated, or one ends up with

$$e_1 e_2 e_3 e_4 \dots e_{2N-2} e_{2N-1} e_{2N-2} \dots e_3 e_2 e_1.$$

But then this can be reduced by using  $e_{2N-2} e_{2N-1} e_{2N-2} = e_{2N-2}$  and so on. Proceeding like this one can eliminate all of them, leaving

$$A = (q + q^{-1})^{\mathcal{N}} \mathcal{B} \quad (\text{B3})$$

where  $\mathcal{N}$  is an integer independent of representation. In fact,  $\mathcal{N}$  is the number of closed loops in the graphical representation of  $\mathcal{L}$ . This proves (B1) and (B2) for any representation of the  $e_i$ , as long as it satisfies the Temperley-Lieb algebra.

For the loop models based on the  $SO(3)$  BMW algebra, the  $e$  in  $\mathcal{B}$  are replaced with  $E$ . The arguments then go through as above.

## APPENDIX C: $E$ , $X$ AND BMW

This appendix collects formulas connected to the  $SO(3)$  BMW algebra. Much of this appendix is discussed in depth in [32], and what is not can be obtained by using these results along with the explicit Boltzmann weights for the  $k = 2$  RSOS models [29].

The generators  $X_i$  and  $E_i$  can be defined in terms of the Temperley-Lieb generators by using the projectors  $\mathcal{P}_i = I - e_i / (q + q^{-1})$  onto the spin-1 representation of  $U_q(\mathfrak{sl}(2))$ , giving [32]

$$\begin{aligned} E_i &= \mathcal{P}_{2i+1} \mathcal{P}_{2i+3} e_{2i+2} e_{2i+1} e_{2i+3} e_{2i+2} \mathcal{P}_{2i+1} \mathcal{P}_{2i+3}, \\ X_i &= (q + q^{-1}) \mathcal{P}_{2i+1} \mathcal{P}_{2i+3} e_{2i+2} \mathcal{P}_{2i+1} \mathcal{P}_{2i+3}. \end{aligned} \quad (\text{C1})$$

Representations of the  $SO(3)$  BMW algebra therefore can be found from representation of the Temperley-Lieb algebra simply by plugging into (C1). In particular, a graphical representation in terms of non-crossing loops can be found from the pictures in figure 7 [32].

The  $SO(3)$  BMW algebra is usually written in terms of  $E_i$  and  $B_i$ , where  $B_i$  is a braiding operator (i.e. satisfies  $B_i B_{i+1} B_i = B_{i+1} B_i B_{i+1}$ ). Here it is convenient to write them in terms of  $I$ ,  $X$ , and  $E$ ; the expression for  $B$  in



terms of these can be found in [32]. The  $E_i$  satisfy the Temperley-Lieb algebra amongst themselves:

$$\begin{aligned} E_i^2 &= (Q-1)E_i, \\ E_i E_{i\pm 1} E_i &= E_i. \end{aligned} \quad (\text{C2})$$

Relations involving the  $X$  are:

$$(X_i)^2 = (Q-2)X_i + E_i. \quad (\text{C3})$$

and

$$\begin{aligned} X_i E_{i+1} X_i &= X_{i+1} E_i X_{i+1}, \\ E_i X_{i+1} E_i &= (Q-1)E_i, \\ X_i E_{i+1} E_i &= X_{i+1} E_i, \\ X_i X_{i+1} E_i &= (Q-2)X_{i+1} E_i + E_i, \\ X_i X_{i+1} X_i - X_{i+1} X_i X_{i+1} &= X_{i+1} E_i + E_i X_{i+1} + X_i \\ &\quad - E_i - X_i E_{i+1} - E_{i+1} X_i \\ &\quad - E_{i+1} + X_{i+1}. \end{aligned}$$

All relations also hold with  $i$  and  $i+1$  interchanged, and with the order of products in each term reversed. All generators labeled by sites  $i$  and  $j$  commute when  $|i-j| > 1$ . It is instructive to use the graphical representation in figure 12 to verify these relations.

Explicit expressions for  $E$  and  $X$  in the  $k=2$  height representation discussed in this paper can be found either by substituting (11) into (C1), or from the explicit Boltzmann weights. Since the  $E_i$  satisfy the Temperley-Lieb algebra, they end up satisfying the identical relation as the  $e_i$ , the only difference being that the heights here are always even, with the adjacency rules in (26) for  $k=2$ . Define  $[a] = \sin(a\pi/(p+1))$ . The  $X_i$  in the height representation are

sentation are

$$h \begin{array}{c} h+2 \\ \diamond \\ h \end{array} h+2 = \frac{\sqrt{[h-1][h+3]}}{[h+1]}$$

$$h \begin{array}{c} h+2 \\ \diamond \\ h+2 \end{array} h+2 = \frac{[h+3]}{[h+1]}$$

$$h \begin{array}{c} h+2 \\ \diamond \\ h \end{array} h = \frac{[h+2][2]}{[h+1][1]}$$

$$h \begin{array}{c} h \\ \diamond \\ h+2 \end{array} h = \frac{[h-1]}{[h+1]} \sqrt{\frac{[h+2]}{[h]}}$$

$$h \begin{array}{c} h \\ \diamond \\ h \end{array} h = \frac{[1]}{[2][h]} \left( \frac{[h-1]^2}{[h+1]} + \frac{[h+1]^2}{[h-1]} \right)$$

The remaining non-zero elements of  $X_i$  are found by either using the symmetry  $h \leftrightarrow p+1-h$ , or by flipping them horizontally or vertically. All others are zero. The fact that the first of these is non-vanishing has a number of interesting consequences discussed in section V.

- 
- [1] B. Nienhuis in *Phase Transitions and Critical Phenomena*, ed. by C. Domb and J. Lebowitz, vol. 11, (Academic Press, 1987).
- [2] H.W.J. Blöte and B. Nienhuis, *Physica A* **160**, 121 (1989); *Phys. Rev. Lett.* **72**, 1372 (1994)
- [3] J.L. Jacobsen and J. Kondev, *Nucl. Phys. B* **532**, 635 (1998) [arXiv:cond-mat/9804048]
- [4] A. A. Belavin, A. M. Polyakov and A. B. Zamolodchikov, *Nucl. Phys. B* **241** (1984) 333.
- [5] V. S. Dotsenko, *Nucl. Phys. B* **235**, 54 (1984).
- [6] for a review accesible to physicists, see J.L. Cardy, *Annals Phys.* **318**, 81 (2005) [arXiv:cond-mat/0503313].
- [7] A.Y. Kitaev, *Annals Phys.* **303**, 2 (2003) [arXiv:quant-ph/9707021]
- [8] M. Freedman, *Comm. Math. Phys.* **234**, 129 (2003) [arXiv: quant-ph/0110060]; M. Freedman, C. Nayak, K. Shtengel, K. Walker and Z. Wang, *Annals Phys.* **310**, 428 (2004) [arXiv: cond-mat/0307511]; M. Freedman, C. Nayak and K. Shtengel, *Phys. Rev. Lett.* **94**, 147205 (2005) [arXiv:cond-mat/0408257].
- [9] E. Bettelheim, I. Gruzberg, A.W.W. Ludwig and P. Wiegmann, *Phys. Rev. Lett.* **95**, 251601 (2005) [arXiv:hep-th/0503013].
- [10] C.M. Fortuin and P.W. Kasteleyn, *Physica* **57**, 536 (1972).
- [11] R.J. Baxter, *Exactly Solved Models in Statistical Mechanics* (Academic, London, 1982).
- [12] P. Fendley and E. Fradkin, *Phys. Rev. B* **72**, 024412 (2005) [arXiv:cond-mat/0502071].
- [13] G.E. Andrews, R.J. Baxter and P.J. Forrester, *J. Stat. Phys.* **35**, 193 (1984).
- [14] V. Pasquier, *Nucl. Phys. B* **285**, 162 (1987).
- [15] H. Temperley and E.H. Lieb, *Proc. Roy. Soc. (London)* **A322**, 251 (1971).
- [16] D.A. Huse, *Phys. Rev. B* **30**, 3908 (1984).
- [17] V. Pasquier, *J. Phys. A* **20**, L1229 (1987).
- [18] P. Di Francesco, H. Saleur and J.-B. Zuber, *Nucl. Phys. B* **285**, 454 (1987); *J. Stat. Phys.* **49**, 57 (1987)
- [19] V.S. Dotsenko and V.A. Fateev, *Nucl. Phys. B* **240**, 312 (1984).
- [20] B. Nienhuis, *Int. J. Mod. Phys. B* **4**, 929 (1990)
- [21] S.O. Warnaar and B. Nienhuis, *J. Phys. A* **26**, 2301 (1993) [arXiv:hep-th/9301026]
- [22] S.O. Warnaar, P.A. Pearce, K.A. Seaton and B. Nienhuis,

- J. Stat. Phys. **74**, 469 (1994) [arXiv:hep-th/9305134].
- [23] P. Fendley, K. Sengupta and S. Sachdev, Phys. Rev. B **69** (2004) 075106 [arXiv:cond-mat/0309438]
- [24] D.A. Huse, Phys. Rev. Lett. **49** 1121 (1982); J. Phys. A **16** 4369 (1983).
- [25] A.B. Zamolodchikov, in *Fields, Strings and Quantum Gravity*, eds H. Guo et al (Gordon and Breach, 1990); Al. B. Zamolodchikov, Nucl. Phys. B **358**, 497 (1991).
- [26] A.B. Zamolodchikov, Mod. Phys. Lett. A **6**, 1807 (1991).
- [27] F.A. Smirnov, Phys. Lett. B **275**, 109 (1992).
- [28] P.P. Kulish, N.Yu. Reshetikhin and E.K. Sklyanin, Lett. Math. Phys. **5**, 393 (1981).
- [29] E. Date, M. Jimbo, T. Miwa and M. Okado, Lett. Math. Phys. **12**, 209 (1986) [Erratum-ibid. **14**, 97 (1987)].
- [30] E. Date, M. Jimbo, A. Kuniba, T. Miwa and M. Okado, Nucl. Phys. B **290**, 231 (1987).
- [31] J. Murakami, Osaka J. Math. **24** (1987) 745; J. Birman and H. Wenzl, Trans. Amer. Math. Soc. **313** (1989) 239.
- [32] P. Fendley and N. Read, J. Phys. A **35**, 10675 (2003) [arXiv:hep-th/0207176].
- [33] L. Chim and A.B. Zamolodchikov, Int. J. Mod. Phys. A **7**, 5317 (1992).
- [34] K. Schoutens, Nucl. Phys. B **344**, 665 (1990).
- [35] A. B. Zamolodchikov, Nucl. Phys. B **366**, 122 (1991).
- [36] P. Di Francesco, H. Saleur and J.-B. Zuber, Nucl. Phys. B **300**, 393 (1988).
- [37] U. Grimm, Lett. Math. Phys. **32** 183 (1994) [arXiv:hep-th/9402094]; U. Grimm and S. O. Warnaar, Nucl. Phys. B **435**, 482 (1995) [arXiv:hep-th/9407046].
- [38] D. Friedan, Z. Qiu and S.H. Shenker, Phys. Rev. Lett. **52**, 1575 (1984).
- [39] J. L. Cardy, Nucl. Phys. B **270**, 186 (1986).
- [40] E. Witten, Commun. Math. Phys. **92**, 455 (1984).
- [41] V.G. Knizhnik and A.B. Zamolodchikov, Nucl. Phys. B **247**, 83 (1984).
- [42] P. Goddard, A. Kent and D. Olive, Phys. Lett. B **152**, 88 (1985); Int. J. Mod. Phys. A **1**, 303 (1986).